AN ABSTRACT OF THE THESIS OF

Kayla Ostrow for the degree of Master of Science in Civil Engineering presented on July 21, 2023.

Title: Performance-Based Design Methodology for Using Emergent Vegetation to Mitigate Wave Overtopping.

Abstract approved: ____

Daniel T. Cox

To facilitate the design of Natural and Nature-Based Features (NNBF) for flood protection, this thesis expands an existing engineering design methodology to NNBF systems. The existing approach is a Level III reliability method for the performance-based design of traditional coastal engineering systems. The expanded methodology incorporates uncertainties inherent to both hydrodynamics and vegetation, producing the expected performance of an NNBF system over its design life. This approach is examined with an idealized case study inspired by a Southern Florida embayment containing a hybrid system with a revetment and mangroves, which are planted at two years old. The relevant vegetation parameters are determined with empirical allometric relations. The expected overtopping and associated probability of failure are calculated in each year of the design life. These performance variables are not constant in time; the probability of failure peaks in the third year of the design life before decreasing, indicating improved performance of the system over time. Alternate design configurations are tested, with more mangroves resulting in better performance of the hybrid system. Other mangrove restoration tactics are examined, with the natural establishment of mangrove propagules resulting in the maximum probability of failure occurring in year 5, but smaller probabilities of failure at the end of the design life. The model is also run considering the structural failure of mangroves, implemented with a fragility function. The incorporation of mangrove mortality results in higher probabilities of failure. The model is verified through examining different allometric relations, values of uncertainty, and fragility functions. The implications of the model assumptions and future work are discussed.

Performance-Based Design Methodology for Using Emergent Vegetation to Mitigate Wave Overtopping

by
Kayla Ostrow

A THESIS

submitted to

Oregon State University

in partial fulfillment of
the requirements for the
degree of

Master of Science

Presented July 21, 2023
Commencement June 2024

Master of Science thesis of Kayla Ostrow presented on July 21, 2023

APPROVED:

Major Professor, representing Civil Engineering

Head of the School of Civil and Construction Engineering

Dean of the Graduate School

I understand that my thesis will become part of the permanent collection of Oregon State University libraries. My signature below authorizes release of my thesis to any reader upon request.

Kayla Ostrow, Author

ACKNOWLEDGEMENTS

This work would not be possible without the encouragement and guidance of many people. First, I would like to thank my advisor, Dan Cox, for all his guidance and support over the last two years. I would also like to thank the committee for this thesis, Andre Barbosa, Tori Tomiczek, and David Bernell, for their time and feedback.

This project has allowed me to learn from and work with incredible collaborators. I would especially like to thank Esteban Biondi, Greg Guannel, and Tori Tomiczek for their help with the state of the practice paper, Paul Branson for allowing me to visit Australia and help with drag coefficients, and Kiernan Kelty for helping with the transition to OSU and the mangrove project.

I am so grateful to the many friends I have made at OSU. I would especially like to thank those in the Cox group: Dylan Sanderson, Mehrshad Amini, Maggie Libby, Sebastiao Figueira, Amina Meselhe, and Kellen Doyle. I would also like to thank everyone in Covell 003 and the rest of the amazing cohort, including Courtney Beringer, Hailey Bond, Nadia Cohen, and Mo Meek.

Finally, thank you to my family for all their love and support, especially my parents Liz and Alec Ostrow, and my sister Amelia Ostrow, who helped with grammar and proofreading.

This thesis contains work supported by the US Army Corps of Engineers through project number W912HZ2120045 and National Science Foundation CBET Grant number 2110439. Any opinions, findings, conclusions, or recommendations expressed in this material are those of the author and do not necessarily reflect the views of the US Army Corps of Engineers or National Science Foundation.

TABLE OF CONTENTS

Page

TABLE OF CONTENTS (Continued)

TABLE OF CONTENTS (Continued)

Page

LIST OF FIGURES

Figure Page

LIST OF FIGURES (Continued)

Figure Page

LIST OF FIGURES (Continued)

LIST OF TABLES

LIST OF APPENDICES

LIST OF APPENDIX FIGURES

LIST OF APPENDIX FIGURES (Continued)

DEDICATION

To my grandparents.

1. Introduction

Natural and Nature-Based Features (NNBF), also known as Engineering With Nature (EWN) and Nature-Based Solutions (NbS), among other names, describes a range of flood protection measures that either utilize or imitate natural features (Bridges et al. 2021). Examples include beach nourishment, coral reefs, and vegetation. In particular, mangroves, a type of emergent vegetation, have been shown to produce flood protection benefits such as the reduction of wave heights, storm surges, and erosion (*e.g.,* Coops et al. 1996; Menéndez et al. 2020; Narayan et al. 2016; Tomiczek et al. 2020). Furthermore, these systems provide benefits beyond their engineering functions, including storing blue carbon (*e.g.,* Alongi 2020; Taillardat et al. 2018) and supporting economic and recreational activities (*e.g.,* Vo et al. 2012). Because of the engineering and additional benefits, there is growing interest in using these systems for flood risk management.

While numerous studies have identified the fundamental mechanisms of how these systems attenuate waves (*e.g.,* Chang et al. 2022; Kelty et al. 2022; Maza et al. 2019), there are barriers to applying these concepts in practice. To illuminate these barriers, Ostrow et al. (2022) conducted a survey with 32 stakeholders across the academic, consulting, government, and nonprofit fields. The most cited engineering need to increase implementation of NNBF systems was engineering design standards, noted by 19 of 32 stakeholders. This finding agreed with similar surveys and observations (Cherry et al. 2018; Close et al. 2017; National Academies of Sciences, Engineering, and Medicine 2022). To complete a design, engineers have typically utilized engineering design manuals, which often give step-by-step procedures, necessary coefficients, range of applicability, and example calculations. Even though there are guidance documents for NNBF projects, no equivalent has been developed for a design manual (Bridges et al. 2021). Therefore, this thesis seeks to develop an engineering design methodology for NNBF systems.

Engineering design methodologies for emergent vegetation require the incorporation of more uncertainties than are included in traditional design. For example, while a seawall may be sized according to a design standard, emergent vegetation inherently changes due to natural ecological processes. There is also no established way to characterize the uncertainty or reliability of NNBF systems (Temmerman et al. 2023). However, a reliability method for performance-based design is already used for traditional coastal engineering projects, such as caisson breakwaters (Goda 2010). To address the above complications, this thesis expands the existing framework for traditional design to emergent vegetation, including the associated uncertainties.

2. Literature Review

2.1. Performance-Based and Reliability Design

Performance-based design (PBD) has been defined as designing a system to meet a set of goals throughout its design life (Aktan et al. 2007). PBD's focus on performance goals has been contrasted with the more widely-used prescriptive design, which bases the design off of known failure thresholds. This method was developed with the underlying assumption that the engineered structure's goals are met by utilizing these failure thresholds. While the prescriptive method has worked well for common structure types, the underlying assumption has not been as applicable for new structure types (Aktan et al. 2007). In the absence of prescriptive design standards, PBD could provide a design methodology for NNBF systems. The performance criteria for PBD has varied based on the required goals for the specific project. For example, in coastal engineering, the importance of a caisson breakwater determined the allowable sliding distance over its design life (Goda 2010; Takahashi et al. 2001).

An engineering methodology for NNBF should consider the vegetation's inherent uncertainties and changes over time. Prescriptive engineering design standards have typically assumed that engineering parameters can be calculated deterministically, utilizing safety factors to account for uncertainty. However, uncertainties have also been accounted for directly with reliability methods, which probabilistically determine engineering parameters (*e.g.,* USACE 2002). Multiple types of reliability methods have been developed. The most robust, Level III methods, have accounted for the probabilistic distributions of input variables (*e.g.,* Goda 2010; USACE 2002).

PBD methodologies have been used in conjunction with reliability design methods (*e.g.,* Goda 2010; Moehle and Deierlein 2004). In coastal engineering, a family of PBD algorithms was developed to characterize the expected sliding distance of caisson breakwaters; an overview of this history was published in Goda (2010). The methodology considered that caisson breakwaters may slide when faced with extreme waves. They failed if they slid too far. The exact wave conditions that a structure will face during its design lifetime cannot be determined during the design process, so a probabilistic generation of these waves was used to calculate an expected sliding distance. That is, an annual storm was selected from an extreme distribution, the sliding distance was calculated considering uncertainty in each of the intermediate steps, and the results were averaged from multiple Monte Carlo simulations (*e.g.,* Hong et al. 2004; Takayama and Ikeda 1993).

While this Level III reliability PBD framework was initially conceived for stationary processes, nonstationary processes were later added. The methodologies developed for nonstationary processes include considering the performance variables as a function of time (Suh et al. 2012), changing the input distributions over time (Mase et al. 2013; Suh et al. 2012), or using scaling relations (Pillai et al. 2019). Other performance variables have been used instead of expected sliding distance, such as overtopping (Chen and Alani 2012; Pillai et al. 2019). To expand this reliability method for performance-based design to emergent vegetation, the wave height attenuation by vegetation and nonstationary conditions within the vegetation itself should be considered.

2.2. Wave Height Attenuation by Vegetation

Temmerman et al. (2023) conceptually divided the factors affecting wave height attenuation by mangroves into three categories: 1) vegetation conditions, 2) hydrodynamic conditions, and 3) the interaction between the two. The following examples illustrate each category. For the same hydrodynamic conditions, more vegetation biomass should lead to better protection from storms. Not all hydrodynamic conditions are affected equally, as wave height attenuation has been found to be larger than surge reduction (Gedan et al. 2011). The interaction between the two parameters is important, as waves that pass through the interconnected prop root system of *Rhizophora sp*. have been shown to experience larger attenuation rates than waves that pass through the trunk (Kelty et al. 2022).

Wave height attenuation by vegetation has been derived considering the force that the vegetation imparts. The force can be expressed with a Morison-type equation assuming the conditions are drag-dominated and neglecting the inertial term:

$$F_D = \frac{1}{2}\rho C_d b_v N u|u| \tag{2.1}$$

where F_D is the horizontal drag force per unit volume, ρ is the fluid density, C_d is the drag coefficient, b_v is the projected area per unit height of each vegetation stem, N is the vegetation stem density, and u is the horizontal orbital velocity. The National Academy of Sciences (1977) determined the transmitted wave height and energy dissipation due to vegetation using linear wave theory, assuming shallow water, and approximating the vegetation as cylinders. Dalrymple et al. (1984) then generalized this result without using a shallow water approximation, and Mendez and Losada (2004) expanded it to random waves on a planar beach defined using the significant wave height and spectral peak period. The wave height decay equation is given by:

$$H_t = \frac{H_i}{1+\beta \Delta x} \tag{2.2}$$

where H_t is the transmitted wave height, H_i is the initial wave height, Δx is the distance between the locations associated with H_i and H_t, and β is a decay coefficient given by Mendez and Losada (2004) as:

$$\beta = \frac{1}{3\sqrt{\pi}} C_d b_v N H_i k \frac{\sinh^3(kah)+3\sinh(kah)}{(\sinh(2kh)+2kh)\sinh(kh)} \tag{2.3}$$

where k is the wavenumber estimated from linear wave theory, h is the water depth, and ah is the submerged vegetation height. Equation (2.3) contains parameters describing both the hydrodynamics and vegetation conditions.

The stem density, projected area per unit height, submerged vegetation height, and drag coefficient are all parameters that require knowledge of the vegetation conditions. The stem density is the number of trees per unit area. The projected area is the surface area perpendicular to the direction of the flow. The submerged vegetation height is the height of the vegetation that is under the mean water level. When the vegetation is emerged, it is equal to the water depth itself. The drag coefficient an empirical coefficient, used in a similar fashion to form drag coefficients in other applications. These parameters can change over time and space, and their changes have been found to impact the wave height attenuation that vegetation can impart over time (Maza et al. 2021).

2.3. Spatial and Temporal Characteristics of Vegetation

As living organisms, vegetation should be treated differently in performance-based design than traditional coastal engineering infrastructure. This thesis focuses on mangroves, which grow in tropical regions and can survive in saltwater environments. The stem density, projected area per unit height, drag coefficient, and submerged vegetation height depend on multiple factors, including environmental conditions, species, and restoration technique. These factors result in vegetation conditions that change in space and time.

Spatial variability by species, genus, or family of mangroves impacts its morphology, and therefore the ability for the mangroves to attenuate waves. For example, the genus *Rhizophora* *sp.*, commonly known as the red mangrove, has large prop root systems that differentiate it from other types of mangroves, such as white and black mangroves. Mangroves have been observed to organize in zones parallel to shorelines (*e.g.,* Snedaker 1982). Multiple typologies of mangrove forests with different characteristics have been identified; an overview of these typologies was presented in in Tomiczek et al. (2021). Twilley et al. (1999) noted that spatial and temporal changes in mangrove restoration projects are linked and classified them into a hierarchy from the smallest spatial and temporal scales to the largest.

Observed natural temporal changes, like growth and decay processes, also affect the vegetation properties relevant for wave height attenuation. As mangroves grow, their diameters, heights, and projected areas increase. Mangroves have been shown to experience self-thinning, in which their stem density decreases as growth occurs (Alongi 2008; Ward et al. 2006). Vegetation mortality reduces biomass, impacting wave height attenuation. Failure has been observed on different time scales; for example, mortality can be immediate during a storm due to wind and wave damage (*e.g.,* Doyle 1995; Jimenez et al. 1985; Silveira et al. 2022). Mortality may also occur months after a storm due to saltwater intrusion, sediment deposits, drowning, and other environmental changes (*e.g.,* Craighead and Gilbert 1962; Jimenez et al. 1985; Radabaugh et al. 2020; Silveira et al. 2022). For example, Radabaugh et al. (2020) found that extensive mangrove mortality occurred between 3 and 9 months after Hurricane Irma in the Florida Keys. Vegetation can also recover after storms, barring any major environmental changes (Krauss and Osland 2020; Taylor et al. 2013).

3. Methods

3.1. Performance-Based Design Framework

The goal of this Level III performance-based design methodology is to produce an evaluation of the performance of an NNBF system in each year and over the entirety of its design life. The performance is defined with respect to an engineering demand parameter, *EDP*. Calculations of the performance depend on the storm and vegetation conditions. These two variables are treated as independent from each other, so the probability of failure of the system in each year is summarized as:

$$P_f = \int_{IM} \int_M P[EDP > edp|IM = im, M = m] f_{IM}(im) f_M(m) dm dim \tag{3.1}$$

where P_f is the probability of failure in a particular year of the design life, *EDP* is the engineering demand parameter with critical threshold *edp*, *IM* is the intensity measure with a specific value of *im*, and *M* is the morphology with a specific value of *m*. Note that *M* and *IM* may be functions of time, resulting in different distributions for each year of the design life and values of P_f. Equation (3.1) is written in the style of performance-based design equations for seismic design (Moehle and Deierlein 2004), with the addition of a parameter for morphology.

The performance-based design methodology for emergent vegetation is presented as a flow chart (Figure 3.1), updated from Ostrow et al. (2023). The methodology follows the flow chart presented in Goda (2010), which was altered and translated from Shimosako and Takahashi (1998), and then modified herein for NNBF as shown by the boxes with the green, dashed borders. The methodology first establishes initial conditions, then generates a random storm event and determines the vegetation in a particular year. The performance variable is then calculated in that year. The process is repeated for each year of the design life to complete one simulation. If desired, a cumulative performance variable can be calculated from the values for each year. Thousands of Monte Carlo simulations, n_{sim}, are carried out, and the results are averaged in each year of the design life to obtain an expected value of the performance variable for each year. The probability of failure is determined by calculating the percent of simulations exceeding a set threshold. To determine confidence intervals around the performance variables, the entire process is repeated for tens to hundreds of sets, n_{set}, of n_{sim} simulations. Each step of the flow chart in Figure 3.1 is described in the following subsections.

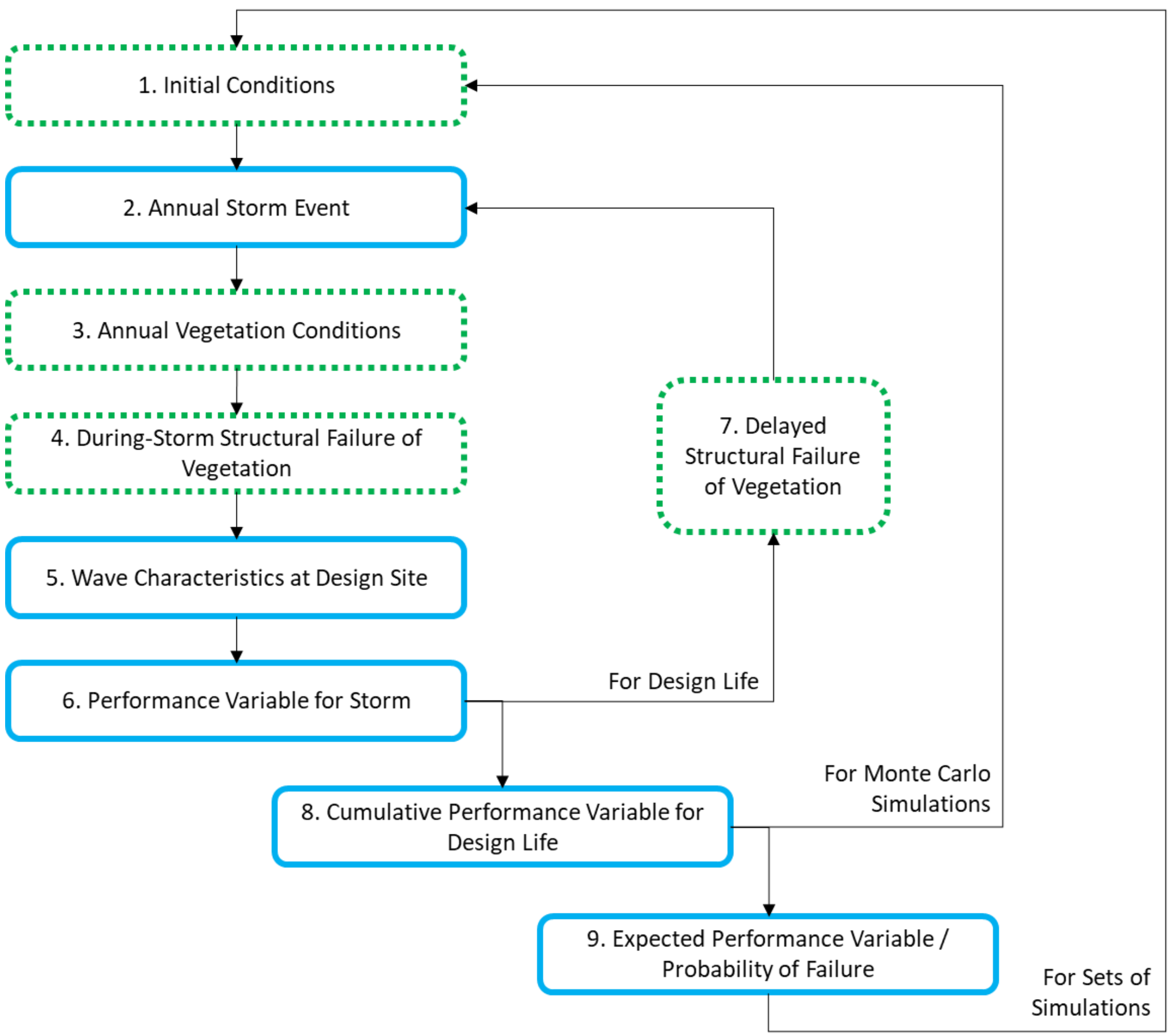

Figure 3.1. Performance-based design methodology for emergent vegetation. Boxes with solid blue outlines are consistent with Goda (2010), and boxes with green dotted lines are added for emergent vegetation.

3.1.1. Step 1. Initial Conditions

The initial conditions of the model should include any parameters relevant to the calculation of the performance variable. The inputs to the model would reflect any design work already completed on the project, for example the 1) performance criteria, 2) bathymetry, 3) wind and wave climate, 4) gray structure, and 5) vegetation conditions. The performance criteria, such as sliding distance or overtopping rate, are used as the engineering demand parameter in Equation (3.1). Limit state functions are defined for each criterion. The model assumes that applicable design guidance has already been applied for the collection of data for the bathymetry and wind and wave climate, and for the design of the gray structure (*e.g.,* USACE 2002). Furthermore, engineers should have already considered applicable design guidance for determining the location, species, and construction methodology for the vegetation (*e.g.,* Bridges et al. 2021). More information about defining the extreme storm conditions is described in Section 3.1.2, and vegetation in Section 3.1.3.

3.1.2. Step 2. Annual Storm Event

The annual storm event is generated from an extreme event distribution. This is the intensity measure in Equation (3.1). The type of extreme event considered depends on the project site and conditions. Typically, PBD methodologies in coastal engineering have used extreme offshore wave heights (*e.g.,* Goda 2010). Other intensity measures can be considered based off of site conditions, such as extreme winds. Relevant hydrodynamic parameters are generated from the extreme storm, including wave heights, periods, and water depths. Aleatory uncertainty is considered in the extreme probability distribution, and epistemic uncertainty is considered in the generation of hydrodynamic parameters.

3.1.3. Step 3. Vegetation Conditions

The vegetation conditions, the morphology parameter in Equation (3.1), should be consistent with the natural vegetation at the project site. For mangroves, parameters such as the hydrology, sediment, and connectivity determine the success of a project (*e.g.,* Piercy et al. 2021). Vegetation grows over time, so the conditions will be different in each year of the design life of the system, and these conditions should be tracked. For example, ecological models have calculated the growth rate of the diameter at breast height in each year to grow the vegetation over time (Berger and Hildenbrandt 2000; Chen and Twilley 1998). In these models, the growth rate in each year depended on ecological parameters such as salinity and temperature, which are multiplied by a maximum growth rate (Chen and Twilley 1998). The initial diameter and associated growth rates depend on the vegetation species and construction of the vegetation patch. For example, planted mangroves have been shown to experience smaller diameter growth rates than natural systems or systems utilizing ecological mangrove restoration (van Bijsterveldt et al. 2022; Xiong et al. 2019). As with the storm conditions, both aleatory and epistemic uncertainties can be considered.

3.1.4. Step 4. During-Storm Structural Failure of Vegetation

Storms may cause trees to fail structurally. Multiple modes of failure may occur, including trunk breakage, overturning of the tree at the root system, and uprooting (*e.g.,* Gijón Mancheño et al. 2022). Structural failure decreases the ability of vegetation to reduce wave heights, as it reduces biomass. To implement this in the model, different limit states can be considered, or damaged vegetation can be removed from the model entirely for conservative design.

3.1.5. Step 5. Wave Transformation

The waves produced in Step 2 are propagated to the design site. This step includes shoaling, refraction, diffraction, reflection, and breaking, as well as energy flux dissipation due to vegetation. These processes can be determined through theoretical or numerical models, and care should be taken to choose a model with the appropriate level of fidelity. The epistemic uncertainty considered in this step could be smaller for higher-fidelity models.

3.1.6. Step 6. Performance Variable for Storm

The performance variable is then calculated with the wave characteristics at the design site. From Step 6, enough information should be obtained to calculate the parameters in the limit state defined in Step 1. Generally, this step will involve empirical equations from engineering manuals, like those for runup, overtopping, and/or wave forces (*e.g.,* Pullen et al. 2007; USACE 2002). Epistemic uncertainty from these empirical equations is considered.

3.1.7. Step 7. Delayed Structural Failure of Vegetation

Vegetation may fail before the next year of the design life. Storms may not just cause failure during the storm, but can cause delayed mortality due to saltwater intrusion, drowning, or other effects (*e.g.,* Craighead and Gilbert 1962; Jimenez et al. 1985; Radabaugh et al. 2020). Large swaths of forest can die due to this process (*e.g.,* Radabaugh et al. 2020). For conservative design, vegetation undergoing delayed mortality can also be removed from the model. After Step 7, Steps 1-7 are repeated for each year of the design life to obtain the value of the performance variable for each year.

3.1.8. Step 8. Cumulative Performance Variable for Design Life

Once the performance variable is obtained in each year, the cumulative sum can be calculated. For example, in the Level III PBD methodology for caisson breakwaters, the cumulative sliding distance was calculated every time the limit state was less than zero; that is, the physical conditions caused the caisson to slide (Goda 2010). This calculation completes one simulation of the performance variable over the design life. Steps 1-8 are repeated to determine the expected performance.

3.1.9. Step 9. Expected Performance Variable and Probability of Failure

Each of the Monte Carlo simulations are averaged to get the expected performance over the design life. This results in one estimation of the: 1) expected performance variable, 2) expected cumulative performance variable, 3) probability of failure due to the performance variable, and 4) probability of failure due to the cumulative performance variable in each year of the design life. The first two estimates are obtained through taking an average of the respective values for each year of the design life. For example, the expected engineering demand parameter in each year t is calculated with the expected value of the engineering demand parameter results from the n_{sim} simulations in each year:

$$EDP_{exp}(t) = E[EDP(t)] \tag{3.2}$$

where $EDP_{exp}(t)$ is the expected engineering demand parameter as a function of time. The probability of failure in each year is equal to the number of simulations that exceed the critical threshold divided by the total number of simulations for the respective values. The probability of failure due to the performance variable is:

$$P_f(t) = E[I(Z(t) < 0)] \tag{3.3}$$

where $P_f(t)$ is the probability of failure in year t, Z is the limit state function, and I is the indicator function. To get confidence intervals around the expected performance over the design life, Steps 1-9 are repeated for a certain number of sets of Monte Carlo simulations. The probability of experiencing at least one failure event during the design life is:

$$P_{Ef} = 1 - \left(1 - P_f(t_0)\right)\left(1 - P_f(t_1)\right)\cdots\left(1 - P_f(T_L - 1)\right) \tag{3.4}$$

where P_{Ef} is the encounter probability and T_L is the length of the design life.

3.1.10. Uncertainty in Parameters

Both aleatory and epistemic uncertainties are considered in the model as described in Sections 3.1.2 through 3.1.6. The values at each step within the model are generated with a normal distribution based upon the expected value from the equation, a bias, and a deviation coefficient (Takayama and Ikeda 1993):

$$\mu_X = (1 + \alpha_X)X_e \tag{3.5}$$

$$\sigma_X = \gamma_X X_e \tag{3.6}$$

where X_e is the value from the equation associated with variable X, α_X is the bias, μ_X is the mean of the error function, γ_X is the deviation coefficient, and σ_X is the standard deviation of the error function. The variable X is then selected from a normal distribution with mean μ_X and standard deviation σ_X. The bias and deviation coefficient are calculated by comparing the measured value of X from experimental data with the estimated value from the relevant equation (Takayama and Ikeda 1993).

$$E\left[\frac{X_M}{X_E}\right] = 1 + \alpha_X \tag{3.7}$$

$$\sqrt{\mathrm{var}\left(\frac{X_M}{X_E}\right)} = \gamma_X \tag{3.8}$$

where X_M is the measured value and X_E is the value from the associated equation for X.

3.2. *Idealized Case Study*

The model was examined with an idealized case study inspired by a coastal embayment in Southern Florida, USA. A hypothetical town in Southern Florida would like to protect its coastal road during storms. The goal of the project was to reduce the overtopping on the coastal road so that motor vehicles can safely traverse the road during storms. The town was considering adding mangroves to the existing revetment to accomplish this goal. Fetch-limited waves were generated over the coastal embayment, so the storm event was defined in terms of the wind speed.

3.2.1. Initial Conditions

This project considered overtopping as the performance variable, as water on the road would reduce vehicle safety. That is, the engineering demand parameter in Equation 3.1 was the overtopping rate, and the limit state function was then (*e.g.,* Pillai et al. 2019):

$$Z(t) = q_c - q(t) \tag{3.9}$$

where q_c is the critical overtopping rate. Critical values of overtopping can be found in Table VI-5-6 of the *Coastal Engineering Manual* (USACE 2002). According to this table, safe driving at all speeds would occur for all overtopping values under $1 * 10^{-6}$ $m^3/s/m$, so this was the value for q_c. The cumulative overtopping that occurred over the design life may also be of use. For illustration purposes, the critical value of cumulative overtopping, $q_{cum,c}$ was set to $1 * 10^{-5}$ $m^3/s/m$. The embayment was modeled as a rectangular basin, with a barrier island on one side and the mainland on the other. The basin had a flat bottom with a 1:30 slope for the last 30 meters on the landward side. The water was 2 m deep over most of the 3 km wide domain, and there was a 3 m high revetment at the landward side protecting the coastal road on the mainland. The proposed mangroves were of the *Rhizophora sp.* genus. A cross-shore width of 20 m of mangroves were considered for design (Figure 3.2), and the alongshore variation in vegetation, bathymetry, and wave conditions was considered uniform.

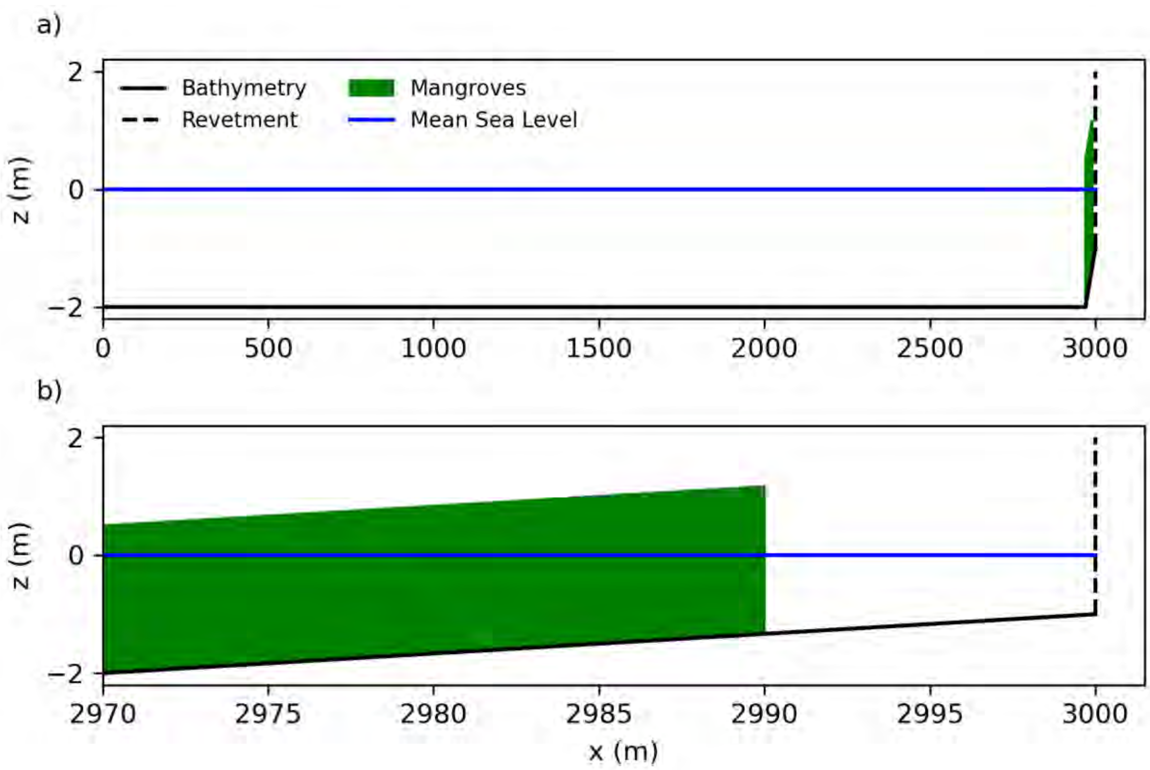

Figure 3.2. Bathymetry for the idealized case study, with a) the entire embayment, and b) the 30 meters encompassing the project site.

3.2.2. <u>Annual Storm Event</u>

The land was sheltered by the barrier island, so fetch-limited waves generated over the length of the embayment were considered. Therefore, the intensity measure in Equation (3.1) was the wind speed at 10 m, *U*. In the *Coastal Engineering Manual*, extreme annual winds can be generated with the Gumbel distribution (USACE 2002):

$$U \sim Gumbel(B, A) \tag{3.10}$$

where B is the location parameter and A is the scale parameter. For an annual storm, it was assumed that the wind speeds lasted long enough to create fetch-limited conditions. The 10-minute average wind speed has been considered to describe stationary conditions, so this value was used to generate the fetch-limited waves (Harper et al. 2010). Annual maximum 2-minute wind speed data from 1996-2022 at the Tampa International Airport was obtained from the National Oceanic and Atmospheric Administration (Lawrimore et al. 2016). The 2-minute wind speeds were converted to 10-minute speeds by dividing by 1.05, the conversion factor for onshore winds at a coastline (Harper et al. 2010). The maximum annual 10-minute wind speeds had a mean of 15.6 m/s and a standard deviation of 2.28 m/s, corresponding to a location parameter of 14.8 and a scale parameter of 1.78 for the fitted Gumbel distribution (Figure 3.3). These values were obtained excluding outliers in the data, as outliers are more likely to represent 2-minute wind gusts that are not maintained for a long enough period to develop fetch-limited waves. These wind speeds may be an overestimation of the 30-45 minute wind durations required to create fetch-limited conditions over this domain (USACE 2002), so they provide a conservative estimate for engineering design. The winds were assumed to be shore normal.

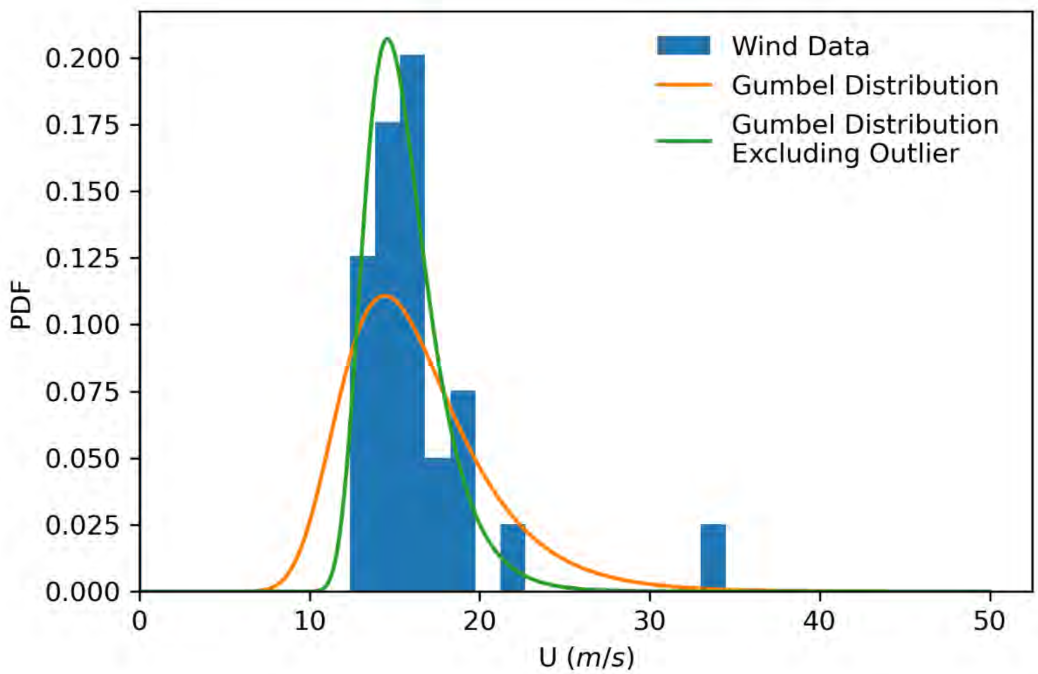

Figure 3.3. Gumbel distribution estimate of 10-minute wind speeds from Tampa, FL.

Hydrodynamic parameters were estimated from the extreme intensity measure distribution. The peak period and significant wave height for fetch-limited waves were calculated from the *Coastal Engineering Manual* using (USACE 2002):

$$T_p = \frac{U_*}{g} 0.651 \left(\frac{gF}{U_*^2}\right)^{\frac{1}{3}} \tag{3.11}$$

$$H_s = \frac{U_*^2}{g} 4.13 * 10^{-2} \left(\frac{gF}{U_*}\right)^{\frac{1}{2}} \tag{3.12}$$

where T_p is the peak period, U_* is the friction velocity calculated from equations II-2-36 in the *Coastal Engineering Manual* (USACE 2002), g is the acceleration due to gravity, F is the fetch length, and H_s is the significant wave height. Surge was also calculated from wind speed with (Silvester 1970):

$$S = \frac{3.3 * 10^{-6} U^2 F}{2gd} \tag{3.13}$$

where S is the surge and d is the water depth without surge. Surge effects of the water body seaward of the barrier island were neglected for this idealized case study.

3.2.3. Vegetation Conditions

Mangrove growth was tracked with diameter, as in the ecological models that use an initial diameter and calculate the growth rate in each year (Chen and Twilley 1998). In the PBD model, the diameter growth rate was approximated by setting a maximum diameter growth rate and selecting a random variable with a uniform distribution:

$$\frac{dD}{dt} \sim unif\left(0, \frac{dD}{dt}_{max}\right) \tag{3.14}$$

where *dD/dt* is the diameter growth rate in each year and dD/dt_{max} is the maximum diameter growth rate. In the absence of mangrove failure, the diameter in each year was calculated by multiplying the time increment, 1 year, by the diameter growth rate in each year and summing the result with the initial diameter in year 0, D_0. Therefore, the random variable controlling the morphology in Equation (3.1) in a specific year *t* was the diameter growth rate summed over the previous years. That is, the parameter *M* was a scaled Irwin-Hall distribution.

The initial diameter and maximum diameter growth rate implemented in the model were determined by construction type. The mangroves were assumed to be planted after two years of growing in a nursery. Typical growth rates for planted mangroves in North America were estimated by Xiong et al. (2019) at 0.33 cm/yr, so the maximum diameter growth rate was set to 0.66 cm/yr to obtain 0.33 cm/yr as the expected value. In the FORMAN ecological model, mangroves experienced mortality from growth suppression if they experienced growth of less than 0.01 cm/yr for two consecutive years (Chen and Twilley 1998; Hurff 2016). The probability of this occurring with a dD/dt_{max} of 0.66 cm/yr was 0.02%. In ecological gap models, the initial diameter of a propagule was 1.3 cm (Chen and Twilley 1998), so the initial diameter for the planted mangroves was assumed to be 2.0 cm.

Once the diameter was obtained, the stem density, projected area, and submerged vegetation height were determined with allometric relations. These empirical relations described the changes in ecological morphology as a function of diameter at breast height. For the allometric relations used in the model, data from published papers were obtained with Web Plot Digitizer (Rohatgi 2022) and regressed with the Python module Statsmodels (Seabold and Perktold 2010). The relation for the drag coefficient was obtained directly from Kelty et al. (2022).

The stem density is the number of stems per unit area. Stem density has been obtained using classical ecological methods, for example counting stems within a set plot size or transect

(Cintrón and Schaeffer-Novelli 1984). Stem density can be described as a function of diameter with the following form (Ward et al. 2006):

$$N = n_1 D^{n_2} \tag{3.15}$$

where n_1 and n_2 are regression parameters. Mangrove systems have been found to experience self-thinning as trees mature, with the stem density decreasing over time (Alongi 2008; Ward et al. 2006). This resulted in a positive n_1 and negative n_2. Stem density as a function of diameter in South Florida was provided by Ward et al. (2006) and Lugo et al. (1980), which was included in the compilation by Jimenez et al. (1985). The regression in the form of Equation (3.15) was calculated from these data and extended to larger diameters. The values for the larger diameters agreed with field data taken from Puerto Rico and Panama (Figure 3.4). Lab studies, which based their stem densities on field data, approximated the data reasonably well.

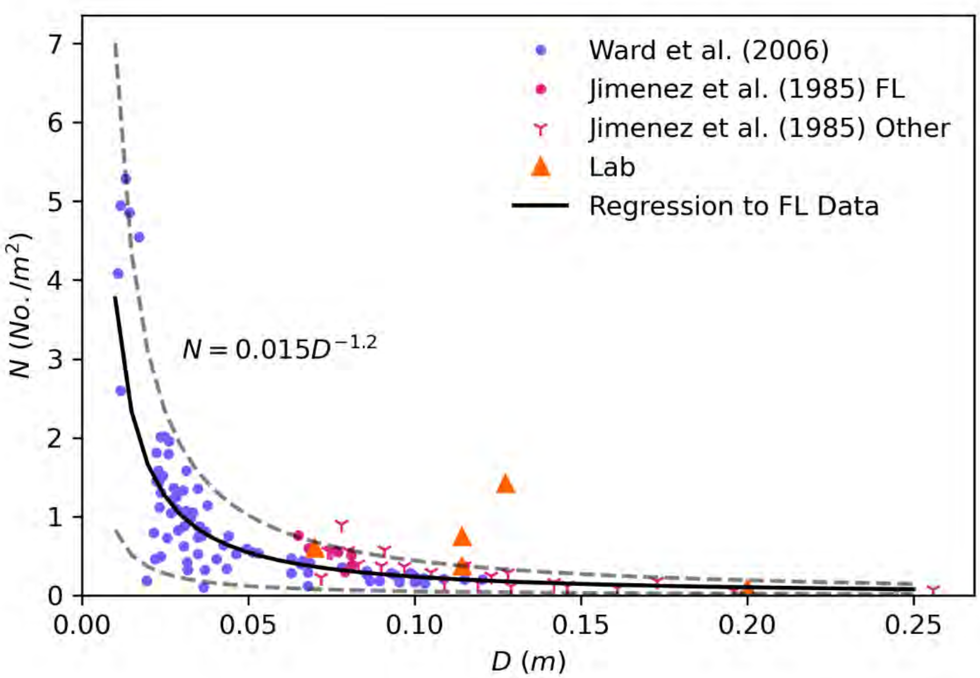

Figure 3.4. Stem density vs. diameter with field data from Florida (Jimenez et al. 1985; Ward et al. 2006), Panama (Jimenez et al. 1985), Puerto Rico (Jimenez et al. 1985), and various lab studies (Bryant et al. 2022; Chang et al. 2022; Kelty et al. 2022; Maza et al. 2019; Wang et al. 2022). The best fit line is calculated with the Florida field data. Dashed lines indicate the mean value plus and minus two standard deviations.

The projected area per unit height has not been commonly used in ecology, but measurement methods have been developed in recent years for engineering purposes. These have included photogrammetry (*e.g.,* Liénard et al. 2016; Maza et al. 2019; Zhang et al. 2015), 3D scanning of individual trees (*e.g.,* Chang et al. 2022), and LiDAR scans of interlocking roots (Kelty et al. 2022). These results have been often reported as projected area per unit height over the relevant area of the mangrove tree(s), and to get b_v, these results were averaged over the submerged vegetation height. For *Rhizophora sp.*, the projected area of the roots has been shown to be larger than the projected area of the trunk, as the tree remains at an approximately constant width over the trunk (*e.g.,* Chang et al. 2022; Kelty et al. 2022). While these methods have provided detailed information at a particular site and time, they have not done so over time. Therefore, for this implementation of the performance-based design methodology, a different method was used: an allometric relation for the projected area of the roots, A_R (Mori et al. 2022; Ohira et al. 2013; Yoshikai et al. 2021).

For *Rhizophora sp.*, the projected area of the roots has been written as a power function (Yoshikai et al. 2021):

$$A_R = a_1 D^{a_2} \tag{3.16}$$

where a_1 and a_2 are regression coefficients. For this allometric relation, A_R starts as a small value, increasing over time as more roots are added and the roots increase in size, resulting in positive values for both a_1 and a_2. There have been two studies that contain projected area as a function of diameter: Mori et al. (2022) and Yoshikai et al. (2021) (Figure 3.5). Mori et al. (2022) contained information about first order roots while Yoshikai et al. (2021) incorporated higher order roots, but the projected area was calculated from the number of roots rather than measured directly. Yoshikai et al. (2021) contained information about larger diameters than Mori et al. (2022), but neither included diameters above 0.15 m. Furthermore, neither included mangroves from Florida. The regression from the Yoshikai et al. (2021) data was used in the model.

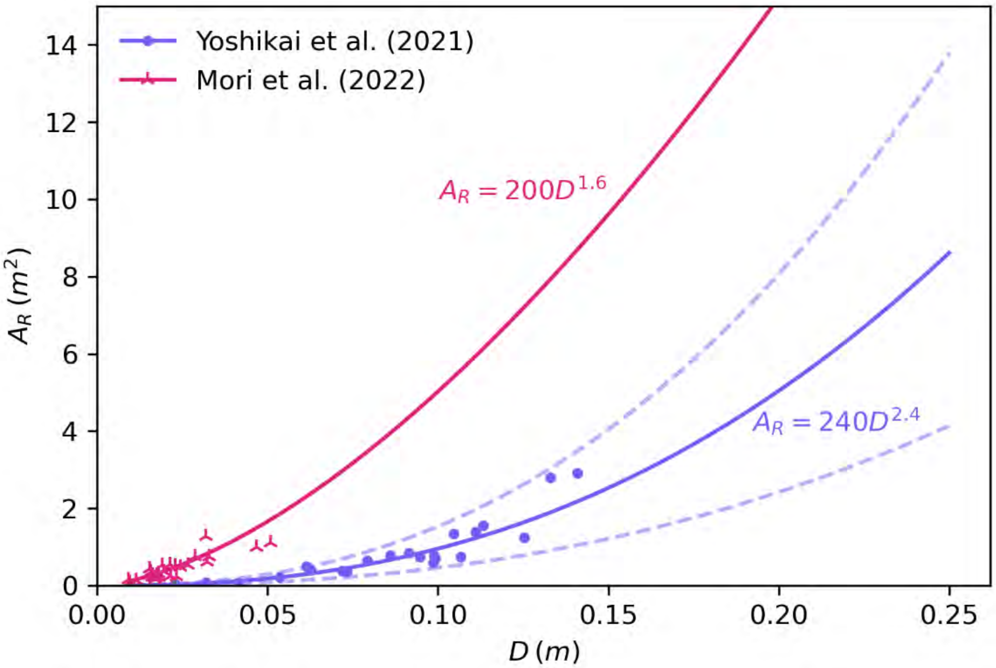

Figure 3.5. Projected area of the roots vs. diameter relations using a regression to the data points from Mori et al. (2022) and Yoshikai et al. (2021). Dashed lines indicate the mean value plus and minus two standard deviations.

With the projected area of the roots given as a function of diameter, the height of the trees, H_T, and height of the roots, H_R, were also required to calculate the projected area per unit height over the entire tree. The height of the trees has been another commonly collected ecological parameter, and H_T and H_R can be collected with clinometers, measuring tapes, and photogrammetry, among other methods (Cintrón and Schaeffer-Novelli 1984; Ohira et al. 2013). The allometric relation for H_T has been commonly represented as quadratic (*e.g.,* Chen and Twilley 1998; Mori et al. 2022) and H_R as linear (Mori et al. 2022; Ohira et al. 2013; Yoshikai et al. 2021):

$$H_T = t_1 + t_2 D + t_3 D^2 \tag{3.17}$$

$$H_R = r_1 + r_2 D \tag{3.18}$$

where t_1, t_2, t_3, r_1, and r_2 are regression parameters. In Equation (3.17), H_T is a concave-down parabola, with positive values for t_1 and t_2 and a negative value for t_3. The allometric relation for H_R increases linearly over time, with positive values for r_1 and r_2. The height of the trees was obtained from Novitzky (2010), who measured diameter and tree heights in Florida. The height of the root system was from Ohira et al. (2013), who used trees in Thailand, and Mori et al. (2022), who measured trees in Japan and Kiribati (Figure 3.6).

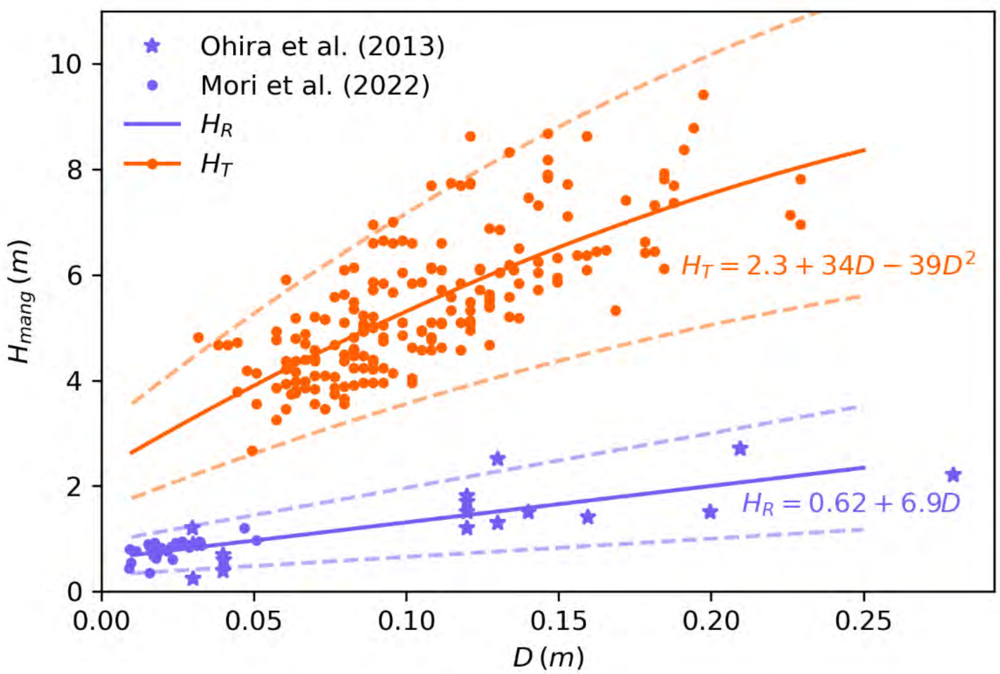

Figure 3.6. Height of mangrove roots and mangrove trees vs. diameter relations and field data. The height of the trees uses data from Novitzky (2010), collected in Florida, and the roots uses Ohira et al. (2013) and Mori et al. (2022), collected in Japan, Kiribati, and Thailand. Dashed lines indicate the mean value plus and minus two standard deviations.

The projected area and submerged vegetation height were obtained with knowledge of the diameter at breast height, projected area of the roots, heights of the tree and roots, and water depth. For this implementation, the entire projected area was calculated and divided by the relevant length scale to get the projected area per unit height. When the vegetation was submerged, b_v was defined as the average of the projected area over the entire tree and *ah* was the height of the trees:

$$b_v = \frac{A_R + (H_T - H_R)D}{H_T} \tag{3.19}$$

$$ah = H_T \tag{3.20}$$

If the water depth was between the top of the roots and top of the tree, only a portion of the trunk was considered for the projected area, and the submerged vegetation height was the same as the water depth:

$$b_v = \frac{A_R + (h - H_R)D}{h} \tag{3.21}$$

$$ah = h \tag{3.22}$$

When the water depth was smaller than the height of the root system, the projected area was a fraction of the total projected area of the roots:

$$b_v = \frac{p_1 A_R}{h} \tag{3.23}$$

where p_1 is a coefficient that determines the proportion of the projected area of the roots that lies underneath the water, given by Mori et al. (2022):

$$p_1 = -0.8\left(\frac{h}{H_R}\right)^2 + 1.8\left(\frac{h}{H_R}\right) \tag{3.24}$$

In this case, ah was also calculated with Equation (3.22). The projected area per unit height could not be smaller than the diameter at breast height.

The drag coefficient has been estimated from a formulation commonly used in laboratory and field experiments. Drag coefficients have been often written in the form:

$$C_d = c_1 + \left(\frac{c_2}{Re}\right)^{c_3} \tag{3.25}$$

where c_1, c_2, and c_3 are regression parameters and Re is the Reynolds number, requiring a characteristic velocity and length scale. The diameter at breast height, the simplest length scale, was used. The wave-induced horizontal velocity at the still water depth plus the surge was used as the characteristic velocity. The relation used in the model was produced by Kelty et al. (2022), which included prototype scale data from Kelty et al. (2022) and rescaled values from Chang et al. (2019) and Maza et al. (2019) (Figure 3.7).

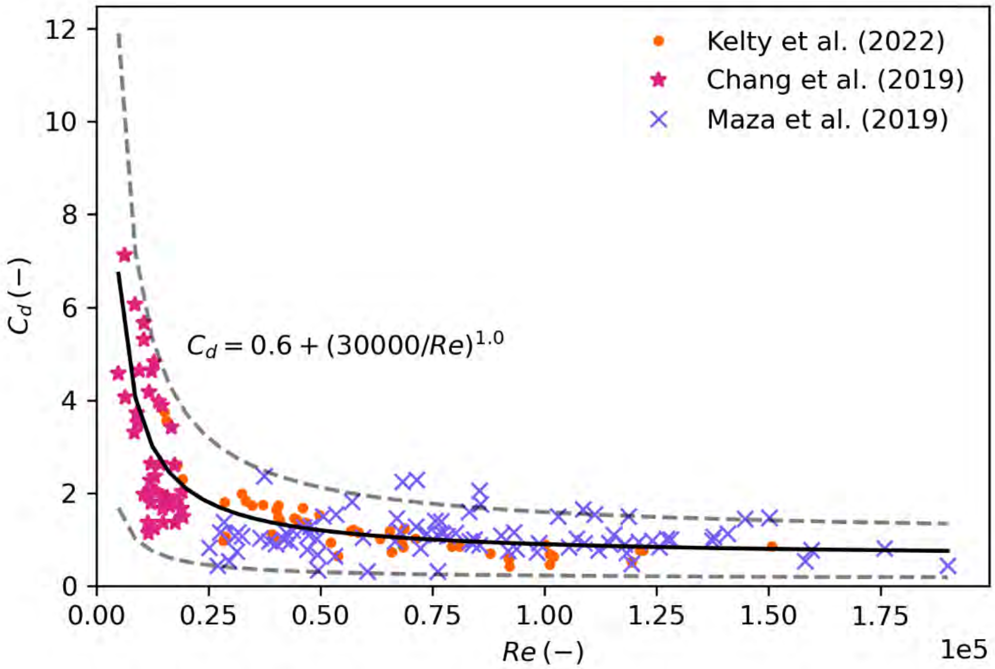

Figure 3.7. Drag coefficient vs. Reynolds number using the best fit line from Kelty et al. (2022), which used data from Kelty et al. (2022) and rescaled data from Chang et al. (2019) and Maza et al. (2019). Dashed lines indicate the mean value plus and minus two standard deviations.

3.2.4. During-Storm Structural Failure of Vegetation

This iteration of the model assumed that the structural failure mode was overturning of the trees (Gijón Mancheño et al. 2022). For a conservative estimate of the performance variable, trees that structurally failed during the storm were removed from the model. A fragility function determined which vegetation was damaged from the storm to the point of failure. In general, fragility functions provide the probability of a certain amount of damage as a function of an intensity measure. One case study in Bangladesh showed that mangroves were able to withstand both trunk breakage and overturning due to wave loads, but not wind loads (Gijón Mancheño et al. 2022). Furthermore, multiple reconnaissance studies in Florida have attributed storm damage to mangroves from wind, rather than waves (Doyle 1995; Radabaugh et al. 2020). While one fragility function has been created for mangrove failure under tsunami loads as a function of overturning moment (Yanagisawa et al. 2009), no fragility function for wind-wave loads has been developed. Therefore, this idealized case study used an estimated fragility function to demonstrate the methodology using wind speed as the intensity measure. The fragility function in the model followed a lognormal cumulative distribution, with a median, θ_f, of 22 m/s and a lognormal standard deviation, β_f, of 0.1 (Figure 3.8). The probability of failure was 1 for a category 1 hurricane, which has a 1-minute sustained wind speed of 33 m/s on the Saffir-Simpson Scale (Schott et al. 2012), equivalent to 30 m/s for a 10-minute wind speed (Harper et al. 2010). Because the fragility function was a placeholder, the results were shown excluding the fragility function unless noted.

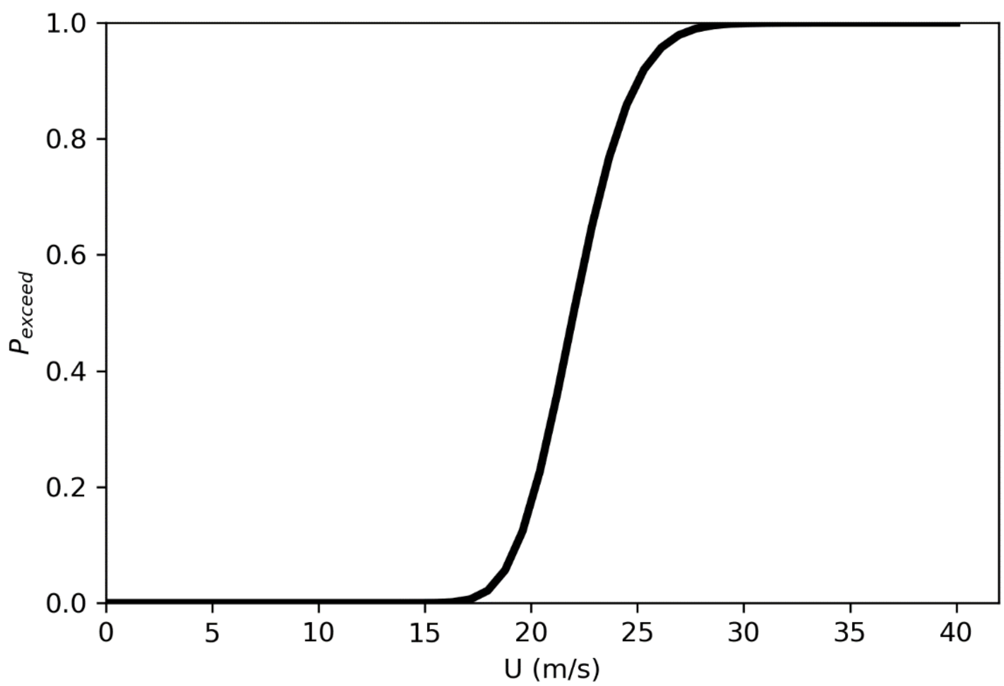

Figure 3.8. Lognormal fragility function for during-storm structural failure of mangroves.

3.2.5. Wave Transformation

The fetch-limited waves were transformed through the mangroves and shoaled on the slope before reaching the revetment. The wave height attenuation through the mangroves was calculated with Equations (2.2) and (2.3), and shoaling was calculated with theoretical equations from Dean and Dalrymple (1984). Both steepness-limited and depth-limited breaking were considered. The maximum wave height to water depth ratio for depth-limited breaking was 0.78, higher than the value of 0.6 considered in the *Coastal Engineering Manual* for fetch-limited waves (USACE 2002).

3.2.6. Performance Variable

The performance variable was the overtopping rate, which occurred over the revetment. The overtopping of a vertical wall with no breaking waves was calculated with the equation in the *Coastal Engineering Manual* proposed by Franco and Franco (1999):

$$\frac{q}{\sqrt{gH_{rev}^3}} = 0.082 \exp\left(-3.0 \frac{R_c}{H_{rev}} \frac{1}{\gamma_B \gamma_S}\right) \tag{3.26}$$

where H_{rev} is the significant wave height at the revetment, R_c is the freeboard, γ_B is a parameter depending on the angle of incidence and differs for short and long-crested waves, and γ_S is a parameter depending on front geometry. This calculation completed the estimation of the overtopping rate for one year of the design life.

3.2.7. Delayed Structural Failure of Vegetation

While delayed mortality is an important consideration for the ability of mangrove systems to attenuate waves, this step was not incorporated in this iteration of the model. Future iterations of the model will include this step as in Section 3.1.7.

3.2.8. Uncertainty in Parameters

The uncertainty in relevant equations was quantified with the bias and deviation coefficient (Table 3.1). The values for the vegetation parameters in Section 3.2.3 were calculated with Equations (3.7) and (3.8). The histograms with these calculations are in Appendix A. All other equations had the base values as in Shimosako and Takahashi (1998) and Hong et al. (2004). For N, H_T, H_R, and A_R, one error value from the standard normal distribution was selected for the entire design life. For all other parameters, one standard normal error value was associated with each year. The standard normal error value was multiplied by σ_X and added to μ_X. To ensure model stability and realistic values, minimum values for each of the generated parameters were applied as in Table 3.1.

Table 3.1. Bias and deviation coefficients and associated sources, and minimum values for each of the parameters containing uncertainty.

Parameter	**Bias, α_X**	**Deviation Coefficient, γ_X**	**Source**	**Minimum Value**
S	0	0.1	Base[1]	0.01 m
H_s	0	0.1	Base[1]	0.05 m
T_p	0	0.1	Base[1]	0.2 s
N	0.04	0.41	Figure A.1	0.01 No./m^2
A_R	0.04	0.28	Figure A.2	0.02 m^2
H_R	0	0.25	Figure A.3	0.1 m
H_T	0.01	0.17	Figure A.4	0.5 m
C_d	0.01	0.38	Figure A.5	0.1
H_t	0	0.1	Base[1]	-
q	0	0.1	Base[1]	-

[1]Values from Shimosako and Takahashi (1998) and Hong et al. (2004).

3.2.9. Alternative Designs

To illustrate the utility of the model, various planting conditions and engineering designs were considered. To look at different mangrove restoration tactics, a scenario in which the propagules were allowed to naturally grow was tested. In this case, the initial diameter was 1.3 cm, the same as the initial diameter in Chen and Twilley (1998). The maximum diameter growth rate was 0.84 cm/yr, with an associated expected value of 0.42 cm/yr (Xiong et al. 2019). Besides the 0 m and 20 m mangrove lengths, other mangrove lengths were considered with the 2-year planting strategy, with x-coordinates of the mangroves in parentheses: 40 m (x = 2,960 m to x = 3,000 m), 80 m (x = 2,920 m to x = 3,000 m), and 160 m (x = 2,840 m to x = 3,000 m).

3.3. Model Implementation

3.3.1. Model Code

The methodology was implemented in Python 3.9.7 using the Spyder IDE. Modules for the hydrodynamics and vegetation were created using the Python packages NumPy (Harris et al. 2020) and SciPy (Virtanen et al. 2020).

3.3.2. Model Grid

A grid was defined within the bounds of the vegetation. This grid allowed for calculations of relevant parameters within the mangrove forest, as different hydrodynamic and vegetation conditions occurred. Multiple grid cell sizes were examined, and a grid convergence study was carried out by comparing the root mean square error of the probability of failure of 1 m, 2 m, 3 m, 4 m, 5 m, 10 m, and 20 m grid cells to a 0.5 m grid cell size. 0.5 m was selected as the lowest resolution due to this being one half the smallest spatial scale associated with tree growth (Twilley et al. 1999). A smaller grid size was expected to correspond to a larger computational time, so the grid size was chosen based on a tradeoff between the root mean square error and computational time. The results are in Appendix B, with a 4 m grid size selected.

3.3.3. Monte Carlo Simulations

As the number of Monte Carlo simulations increased, both the accuracy of the result and computational time to complete the simulations increased. Therefore, a tradeoff between the accuracy and computational time existed, and both metrics were used to determine the number of Monte Carlo simulations. The accuracy was quantified by the coefficient of variation, defined as the standard deviation of the simulations divided by the mean. The coefficient of variation was calculated for the overtopping rate in each year of the design life and averaged to obtain one value. The coefficient of variation was determined for 100, 1,000, 10,000, 100,000, and 1,000,000 simulations. The coefficients of variation for the smaller numbers of simulations were compared to 1,000,000. 10,000 simulations was selected, as this value had a coefficient of variation of over 90% of the value for 1,000,000 simulations while having a small computational time. Appendix C contains the full analysis.

For confidence intervals around the estimates of the performance variables, the entire process in Figure 3.1 was repeated for sets of simulations. The number of sets of simulations was also determined by computational time and accuracy defined by the coefficient of variation. In this case, the coefficient of variation was calculated for both the expected overtopping rate and probability of failure. 100 sets of 10,000 simulations was selected, with the full analysis also in Appendix C.

3.3.4. Hydrodynamic Assumptions

The hydrodynamics were simplified for the model implementation. Equation (3.13) assumed that the surge was formed over a constant depth, which was a good approximation for the case study's bathymetry. Equations (3.11) and (3.12) came from the *Coastal Engineering Manual* (USACE 2002), and depth-limited breaking was modified to use a maximum wave height to water depth ratio of 0.78. Linear wave theory was assumed for the calculations. The wavenumber was calculated with the approximation of Simarro and Orfila (2013). The maximum horizontal wave velocity at the still water level plus surge calculated at the seaward edge of the mangroves was used as the characteristic velocity for the Reynolds number. Reflection was not incorporated, and shoaling was assumed to not occur within the mangroves because energy flux was not conserved. The annual storm was considered to occur at the same tide level in each year. The overtopping in Equation (3.16) required assuming short crested waves and a plain impermeable wall. For a discussion on the implications of these assumptions, see Section 5.3.

3.3.5. Vegetation Assumptions

The model also employed simplifications to the vegetation dynamics. Complicated ecological dynamics were simplified with a randomly selected diameter growth rate and allometric relations. The uniform distribution for dD/dt approximated Equation 14 from Chen and Twilley (1998). The FORMAN model tracked the height of the trees with an equation of the form of Equation (3.5) (Chen and Twilley 1998). To approximate this with uncertainty, one random value from a standard normal distribution was selected for the entire design life for N, H_T, H_R, and A_R. For the height of the trees and roots and the projected area of the roots, this meant that these values could not unexpectedly shrink within the design life. Furthermore, the height of the trees could not be smaller than the height of the roots, so if this occurred, H_T was set to equal H_R. The stem density curve approximated the random addition of propagules and death of mangroves in the FORMAN model (Chen and Twilley 1998). C_d did not face the same restrictions as the other mangrove parameters, as it not only depended on the vegetation, but also on the hydrodynamics. So, one uncertainty value from the standard normal distribution was selected for each year of the design life. The parameter p_1 may vary based on species, but it was used without uncertainty because the relation had a high fit to the data and it was constrained between 0 and 1 (Mori et al. 2022). The canopy was not considered for conservative design. The implications of these assumptions are also discussed in Section 5.3.

3.4. Model Verification

3.4.1. Allometric Relations

The effect of changing the mangrove parameters was determined by running the model with different values of the vegetation parameters. For each of the vegetation parameters in Table 3.1, N, C_d, H_T, H_R, and A_R, the value from the allometric relation and two standard deviations above and below the mean value were considered. The mean and standard deviations were calculated as in Equations (3.5) and (3.6). These values were plotted as the dotted lines in Figures Figure 3.4 through Figure 3.7. The model was considered without uncertainty for this sensitivity test.

3.4.2. Uncertainty in Parameters

The effect of changing the bias and deviation coefficient parameters in Table 3.1 was examined, as in Shimosako and Takahashi (1998). For each of the ten variables in Table 3.1, combinations of biases of -0.1, -0.05, 0, 0.05, and 0.1 and deviation coefficients of 0, 0.1, 0.2, 0.3, and 0.4 were examined. These ranges were similar to the ones in Shimosako and Takahashi (1998) for wave parameters. The deviation coefficients tested went up to 0.4 because these were the highest values seen in the vegetation parameters.

3.4.3. During-Storm Structural Failure of Vegetation

The effects of changing the median and lognormal standard deviation parameters in the fragility function were examined. Fragility functions with θ_f of 20 and 24 m/s, as well as β_f of 0.05 and 0.15 were tested (Figure 3.9).

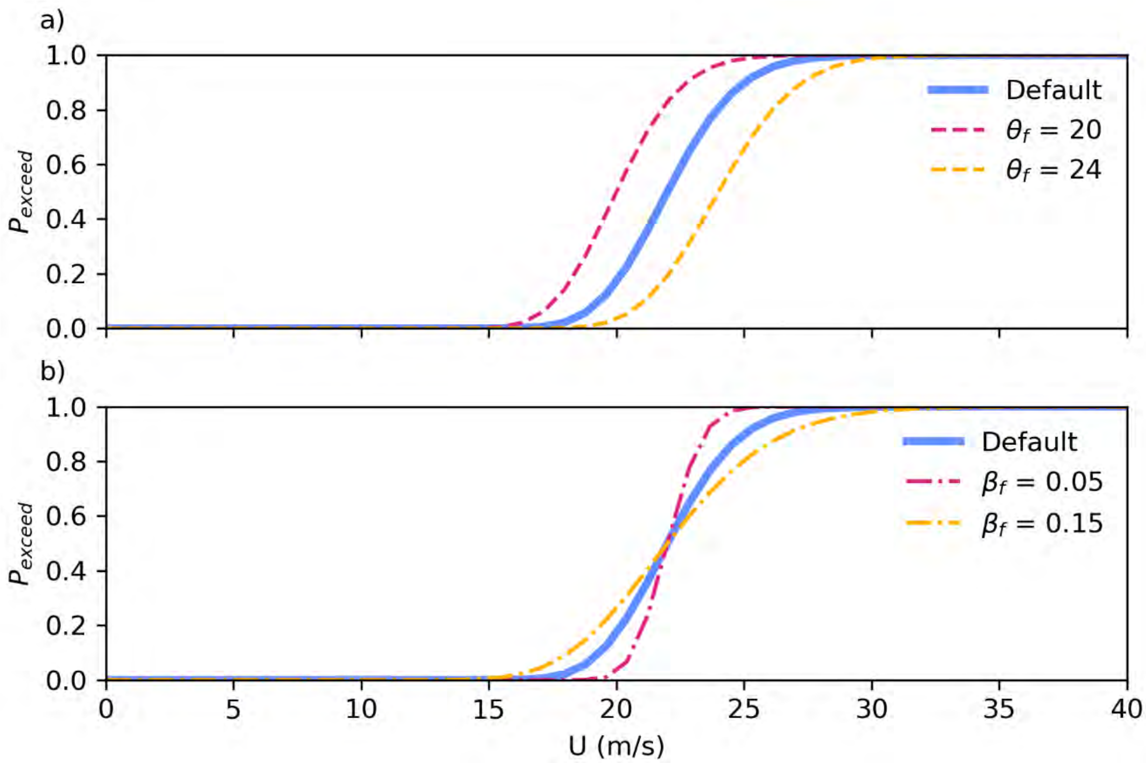

Figure 3.9. Input fragility functions for sensitivity analysis, with a) changes in the median value and b) changes in the logarithmic standard deviation.

4. Results

4.1. Expected Performance of Engineering Designs

4.1.1. Without Mangroves

Without mangroves, the expected overtopping rate was constant over the design life (Figure 4.1). The expected overtopping remained at approximately 2.9 * 10^{-7} $m^3/s/m$ throughout the design life (Figure 4.1a). This was below the failure criterion of 1 * 10^{-6} $m^3/s/m$, but because there was variability due to uncertainties in the input, the resulting probability of failure in each year was 0.049 (Figure 4.1c). However, the probability that there would be at least one failure event over the 50-year design life was P_{Ef} = 91.9% as calculated by Equation (3.4). This could be considered an unacceptable level of risk. The cumulative overtopping rate was approximately a straight line because the overtopping rate was constant and ranged from 2.4 * 10^{-7} $m^3/s/m$ to 1.2 * 10^{-5} $m^3/s/m$ (Figure 4.1b). The probability of failure due to cumulative overtopping increased over the design life, from 0.0052 to 0.40 (Figure 4.1d).

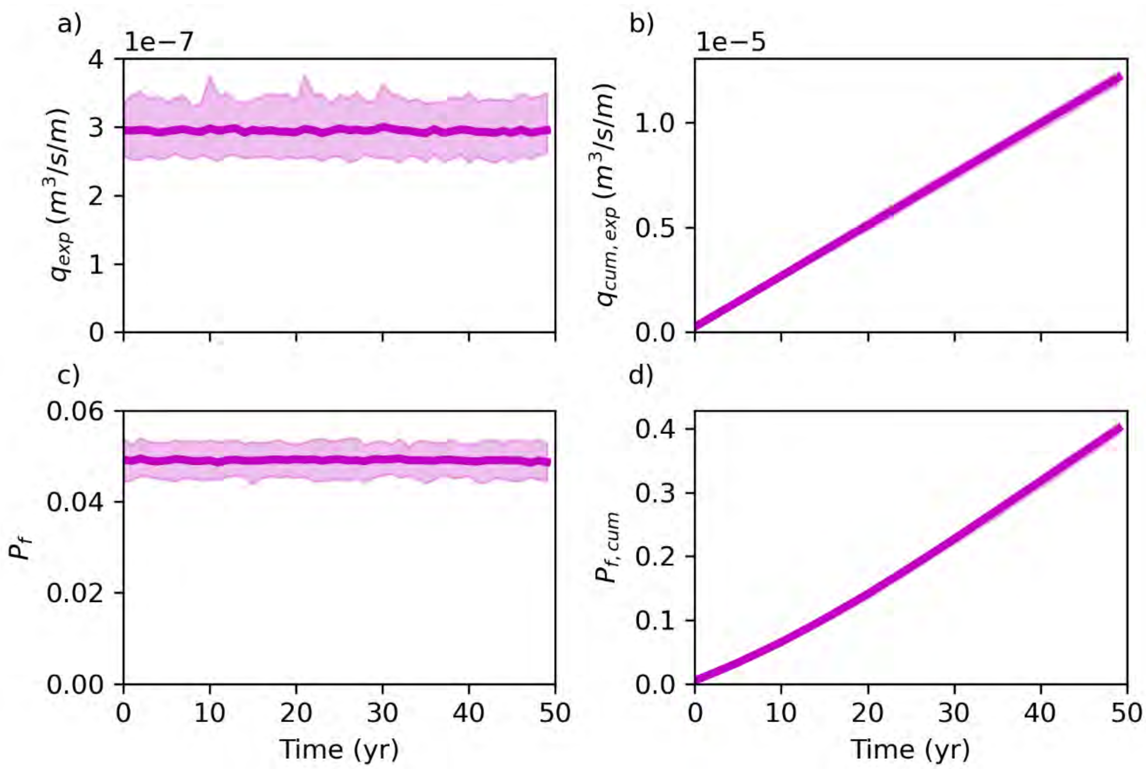

Figure 4.1. Expected performance of the revetment system in the absence of mangroves, with a) the expected value of overtopping, b) the expected cumulative overtopping, and c) the probability of failure due to overtopping, d) the probability of failure due to cumulative overtopping, with 95% confidence intervals.

The hydrodynamics for one set of 10,000 simulations were examined at the beginning of the slope at x = 2,970 m and at the revetment at x = 3,000 m. At x = 2,970 m, 4.93% of waves were breaking, and at x = 3,000 m, 9.29% of waves were breaking, all due to steepness-limited conditions. The waves produced by the model were predominantly Stokes waves (Figure 4.2). The waves were either in intermediate or deep water and did not reach shallow water. Waves at x = 3,000 m had higher significant wave height to water depth ratios than at x = 2,970 m, while having smaller water depth to peak wavelength ratios. For the set of 10,000 simulations shown in Figure 4.2, the shoaling coefficient ranged between 0.94 – 1.04, with a mean of 0.95.

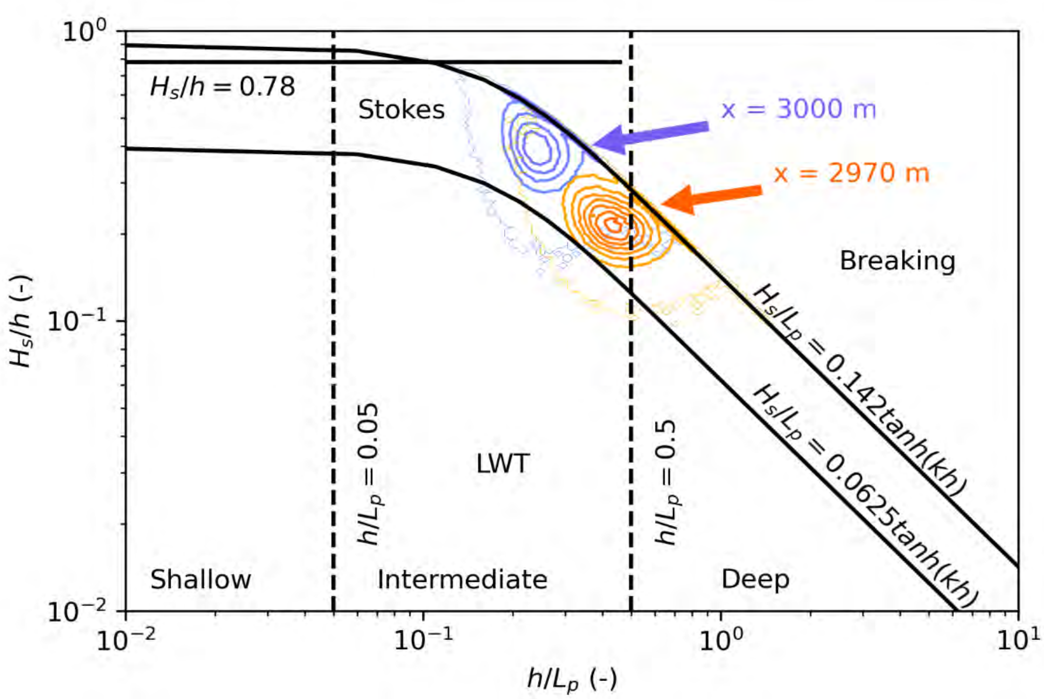

Figure 4.2. Wave conditions for the no mangrove case. The contour plots consist of 200 bins on each axis, and contours indicate increases of 500 counts.

4.1.2. With Mangroves

Including mangroves in the design led to different performance results (Figure 4.3). With mangroves, the system performed better, with the expected overtopping reduced by between 29% and 65% to between 2.1 * 10^{-7} m^3/s/m and 1.0 * 10^{-7} m^3/s/m (Figure 4.3a). The probability of failure in each year was reduced by between 31% and 68% to between 0.034 and 0.015 (Figure 4.3c). The reduced cumulative overtopping ranged from 1.7 * 10^{-7} m^3/s/m to 6.4 * 10^{-6}

m^3/s/m (Figure 4.3b), and the probability of failure for cumulative overtopping decreased to between 0.0036 and 0.18 (Figure 4.3d). Unlike the case with no mangroves, the probability of failure was not constant. The maximum probability of failure occurred in year 3 and decreased in later years. The encounter probability of failure was smaller than the case with no mangroves, at 71.2%. The number of breaking waves at x = 2,970 m was the same as the case with no mangroves, 4.93%, but reduced to 2.6% at x = 3,000 m. Like the no mangrove case, all breaking waves were steepness-limited.

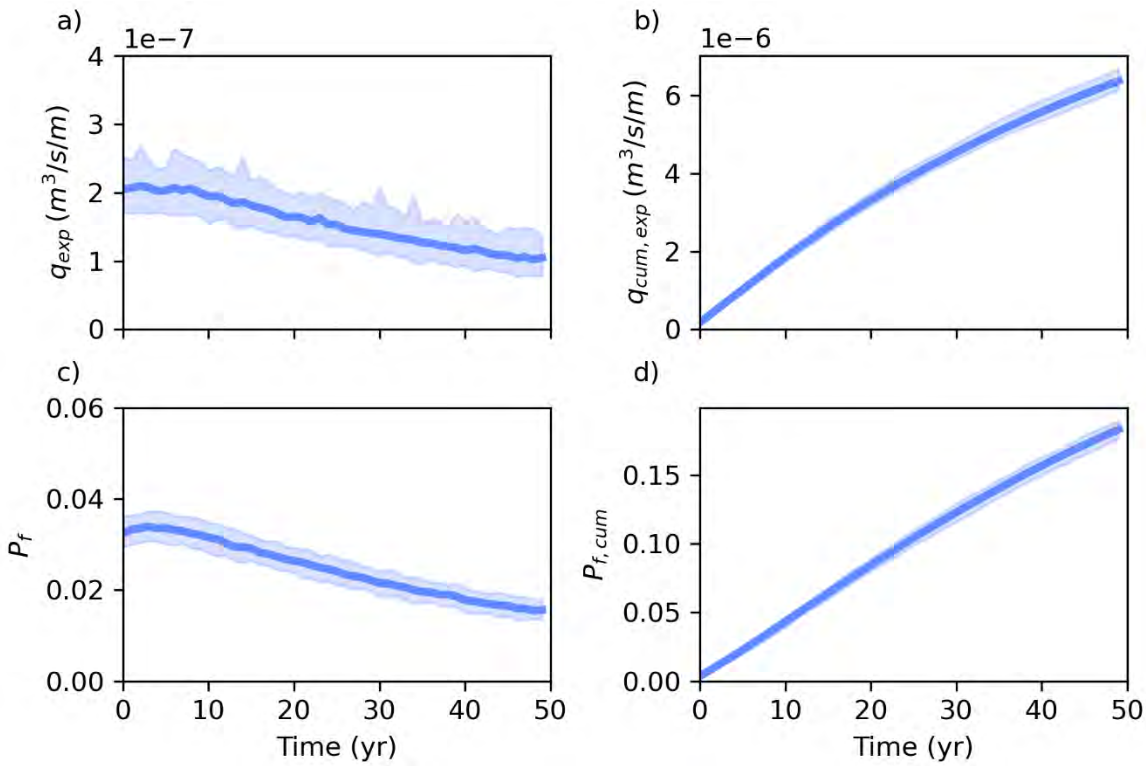

Figure 4.3. Expected performance of the mangrove system for each year of the design life, with a) the expected value of overtopping, b) the expected cumulative overtopping, c) the probability of failure due to overtopping, and d) the probability of failure due to cumulative overtopping with 95% confidence intervals.

The shape of the probability of failure curve reflected the shape of the decay coefficient, β, from Equation (2.1) (Figure 4.4). The decay coefficient was the smallest in the beginning of the design life, with a mean value of 0.0051 m^{-1} in year 4, and a maximum value of 0.0116 m^{-1} in year 49 (Figure 4.4e). Within one set of 10,000 simulations, the 95% confidence interval ranged from 0.0020 m^{-1} to 0.028 m^{-1}, an order of magnitude difference. The stem density, drag coefficient, projected area per unit height, and submerged vegetation height all contributed to the wave height decay coefficient. The stem density and drag coefficient both decreased with time, with the mean of stem density decreasing from 1.72 No./m^2 to 0.12 No./m^2 (Figure 4.4a) and drag coefficient from 2.49 to 0.81 (Figure 4.4c). The projected area per unit height increased with time, from 0.023 m^2/m at the beginning of the design life to 2.27 m^2/m at the end (Figure 4.4b). The 95% confidence intervals for these parameters increased as the values increased, consistent with Equation (3.6). The submerged vegetation height did not change over the design life, staying at a constant 1.79 m (Figure 4.4d).

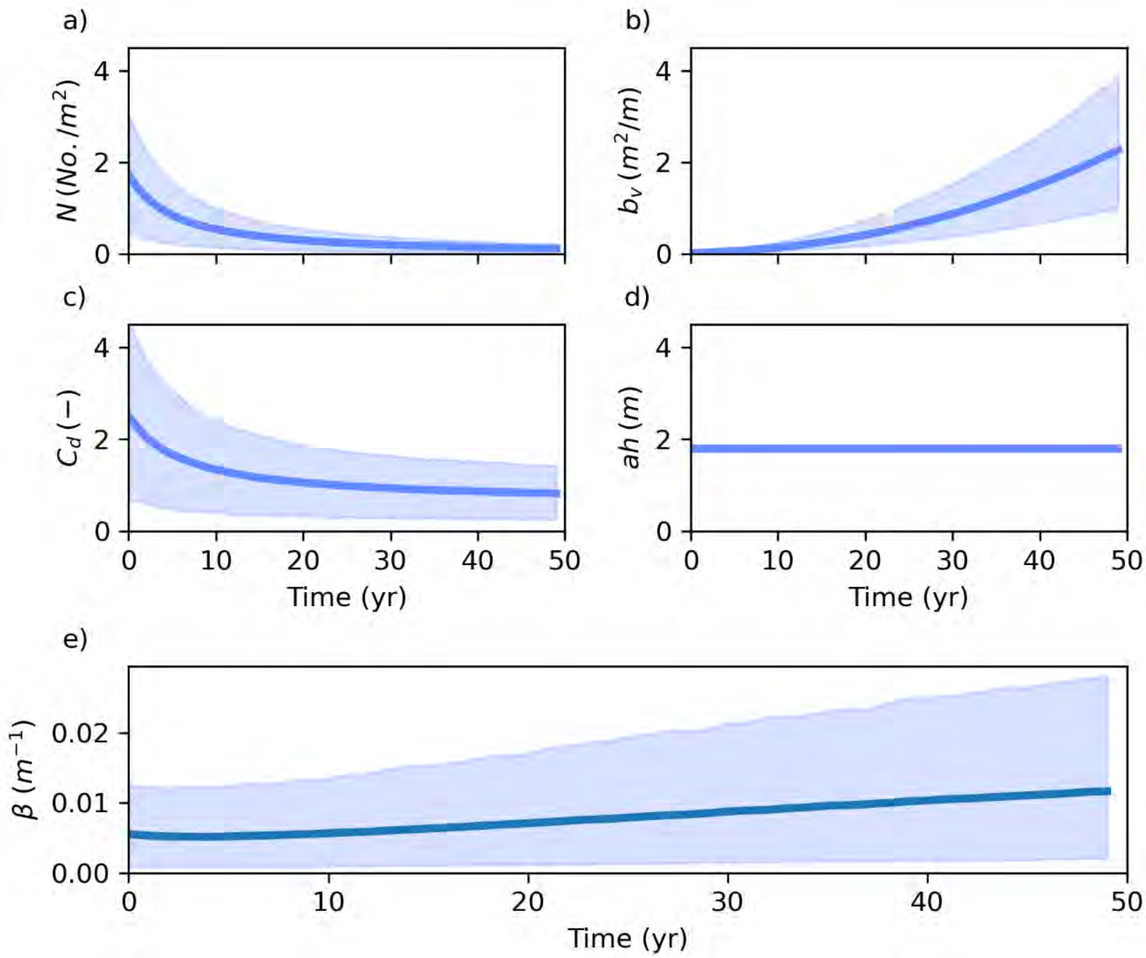

Figure 4.4. Important morphological parameters a) stem density, b) projected area per unit height, c) drag coefficient, and d) submerged vegetation height, with e) the decay coefficient in Equation (2.1) as a function of design life for one set of 10,000 simulations. Each parameter is averaged over the 20 m of mangrove trees and 95% confidence intervals are shown.

4.1.3. Alternative Designs

When allowing natural restoration of the mangroves by starting with propagules, the performance metrics differed from the planted case (Figure 4.5). The maximum probability of failure in this case was 0.034, which was the same as the planted case (Figure 4.5c). The probability of failure at the end of the design life was slightly smaller than for the planted case, with 0.013 instead of 0.015. This led to a smaller encounter probability of failure of 68.5%. The shape of the expected overtopping and probability of failure curves were different, as there was a visible decrease in both curves at the beginning of the design life compared to the planted case. The maximum probability of failure occurred in year 5, rather than year 3.

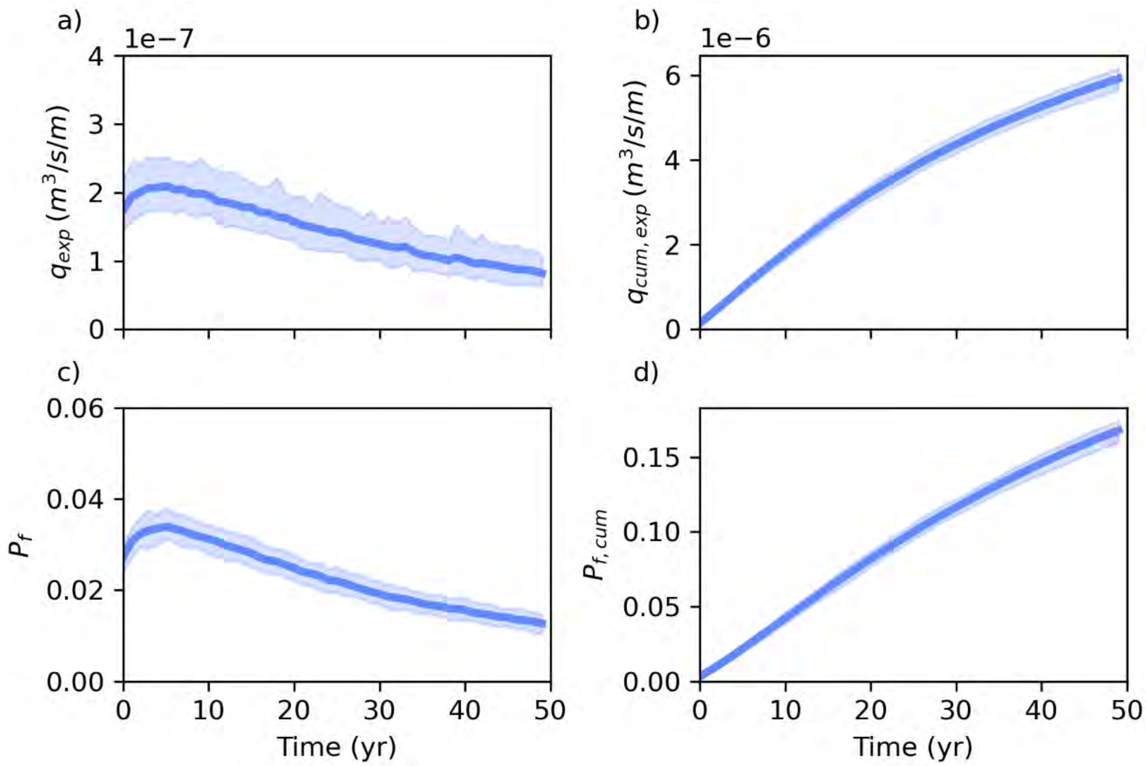

Figure 4.5. Expected performance of the mangrove system when starting from propagules for each year of the design life, with a) the expected value of overtopping, b) the expected cumulative overtopping, c) the probability of failure due to overtopping, and d) the probability of failure due to cumulative overtopping with 95% confidence intervals.

The different initial vegetation conditions resulted in different allometric relations (Figure 4.6). The propagule case resulted in a higher stem density and drag coefficient at the beginning of the design life and a smaller value at the end of the design life with respect to the 2-year planted case (Figure 4.6a and Figure 4.6c). The differences were more pronounced at the beginning of the design life. The opposite was true for the projected area, which became larger for the propagule case than the 2-year planted case (Figure 4.6b). The submerged vegetation height was the same in both cases (Figure 4.6d).

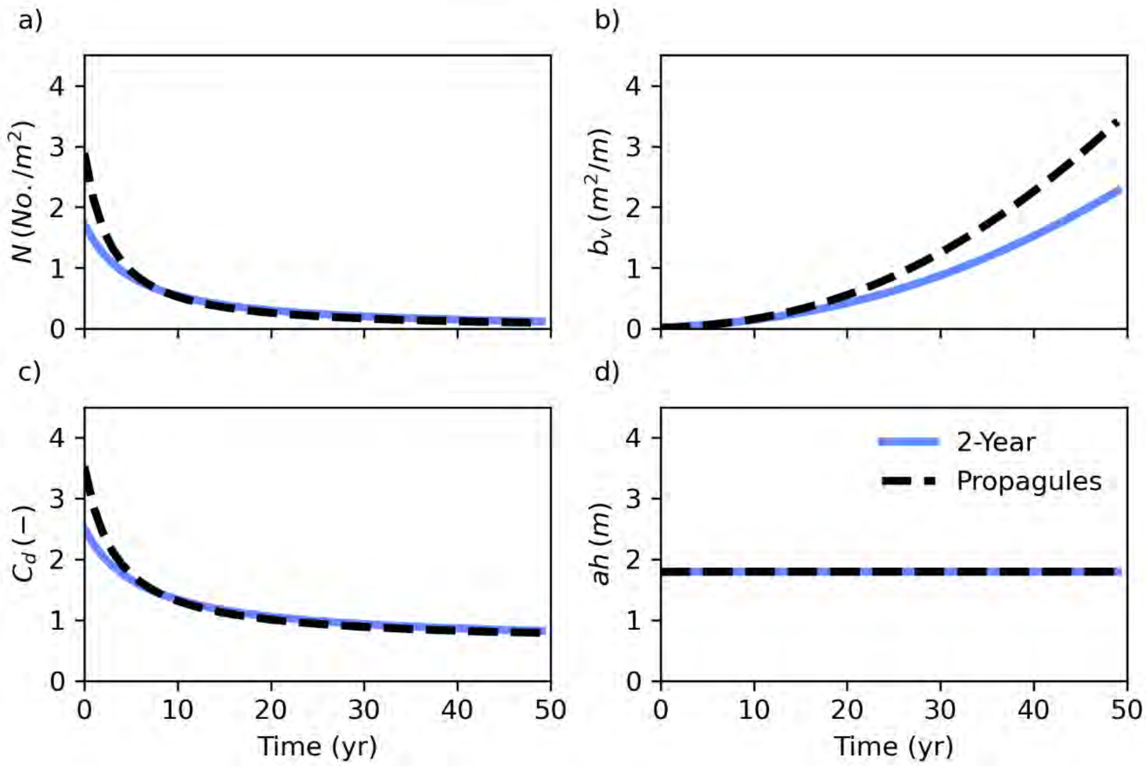

Figure 4.6. Important morphological parameters a) stem density, b) projected area per unit height, c) drag coefficient, and d) submerged vegetation height for the case with planting 2-year mangroves and utilizing propagules averaged for 100 sets of 10,000 simulations.

As more mangroves were added to the system, the encounter probability of failure decreased, indicating an improvement of the performance of the system (Figure 4.7). Without mangroves, P_{Ef} was 91.9%, which may be too high for the design requirements. Adding in 20 m of mangroves reduced this value to 71.3%. This value was further reduced when adding in 40 m, 80 m, and 160 m, with 160 m of mangroves having a P_{Ef} of 7.0%.

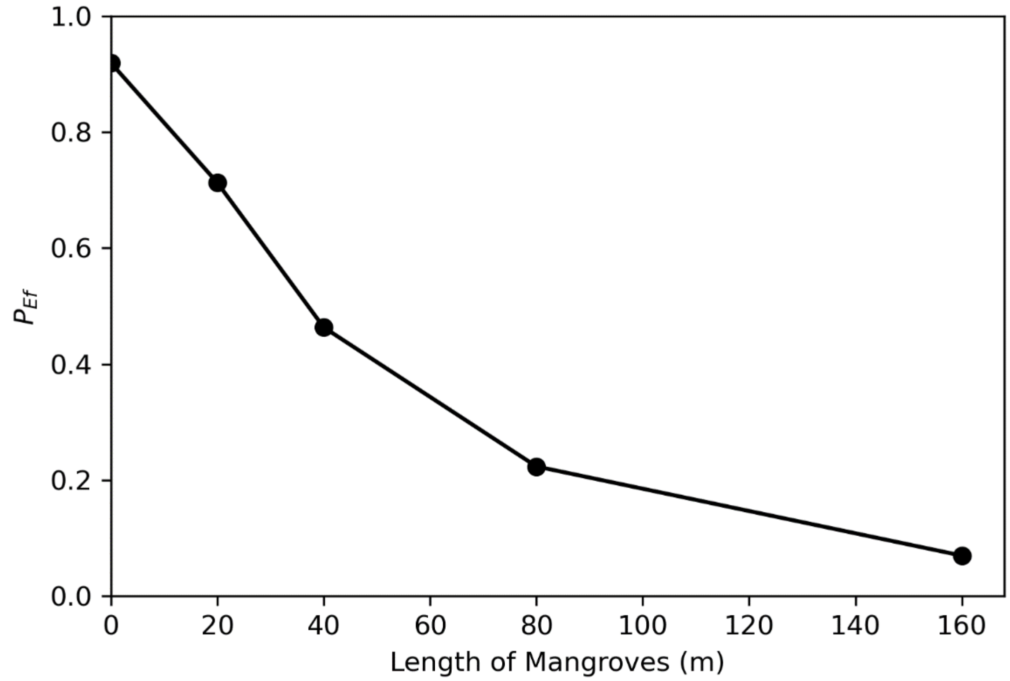

Figure 4.7. Encounter probability of failure as a function of the length of mangroves in the model.

4.1.4. Including During-Storm Structural Failure of Vegetation

Including during-storm structural failure of vegetation (Step 4) resulted in different performance variable results over the design life (Figure 4.8). While the overall performance was still better than the no mangrove case, the performance metrics were worse than when excluding Step 4. The expected overtopping ranged between $2.1 * 10^{-7}$ $m^3/s/m$ and $2.5 * 10^{-7}$ $m^3/s/m$ (Figure 4.8a) and the probability of failure ranged between 0.030 and 0.038 (Figure 4.8c), a smaller range of values than in the case excluding Step 4. The expected value of cumulative overtopping increased from $2.1 * 10^{-7}$ $m^3/s/m$ to $9.9 * 10^{-6}$ $m^3/s/m$ (Figure 4.8b) and the associated probability of failure from 0.005 to 0.38 (Figure 4.8d). The encounter probability was 81.7%, lying in between the no mangrove case and the case without Step 4. The percent difference between the probability of failure with and without Step 4 was 10.8% in year 3 and 62.8% at the end of the design life.

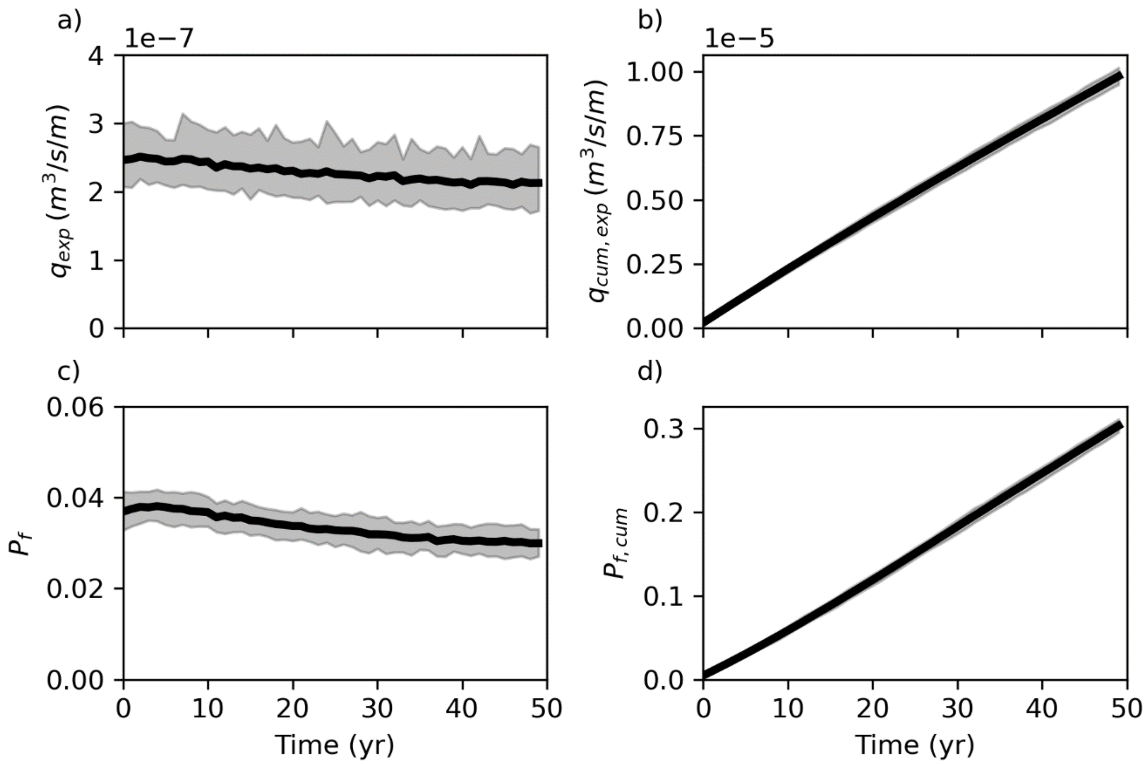

Figure 4.8. Expected performance of the mangrove system when including during-storm structural failure of vegetation, with a) the expected value of overtopping, b) the expected cumulative overtopping, c) the probability of failure due to overtopping, and d) the probability of failure due to cumulative overtopping with 95% confidence intervals.

The average vegetation parameters used in Equation (2.3) differed from the case without Step 4 (Figure 4.9). When including Step 4, the stem density and drag coefficients did not decrease by the same amount, with the average stem density reaching a minimum value of 0.43 No./m^2 instead of 0.12 No./m^2 (Figure 4.9a), and drag coefficient having a minimum of 1.18 instead of 0.82 (Figure 4.9c). The projected area per unit height did not increase as much as it did without Step 4, reaching an average of 0.96 m^2/m instead of 2.27 m^2/m (Figure 4.9b). The submerged vegetation depth was the same in both simulations (Figure 4.9d).

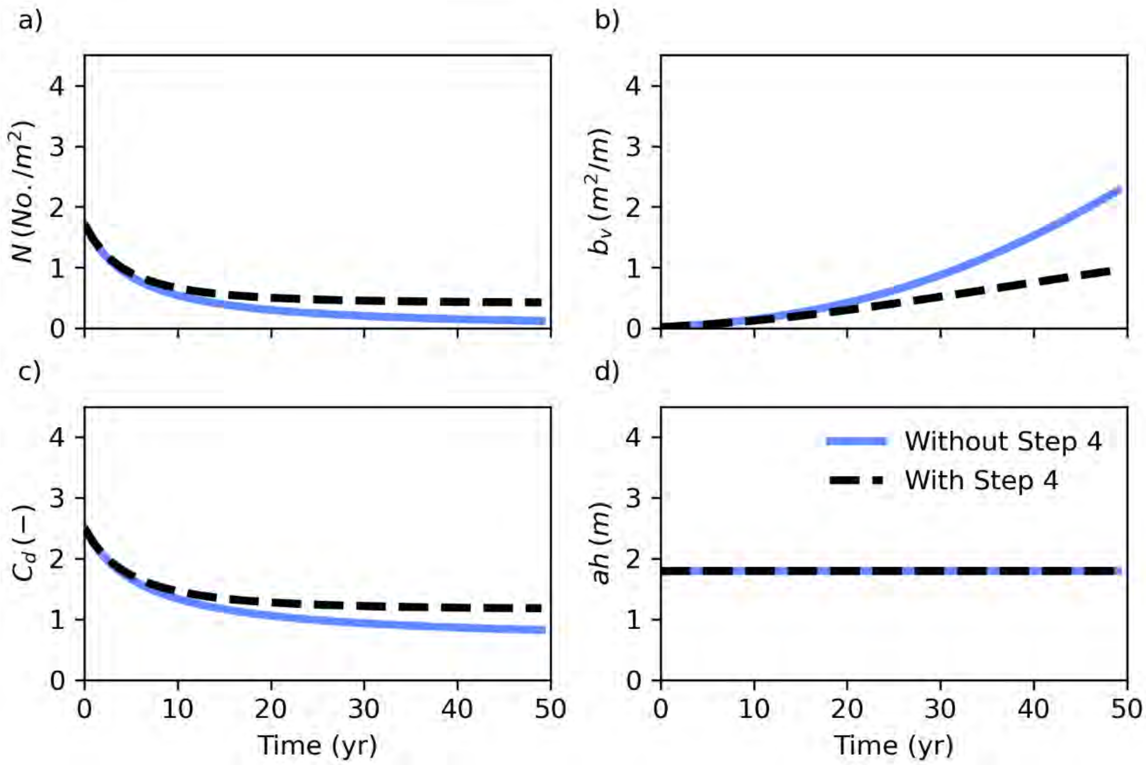

Figure 4.9. Important morphological parameters a) stem density, b) projected area per unit height, c) drag coefficient, and d) submerged vegetation height for the cases without Step 4 and with Step 4 in Figure 3.1 averaged for 100 sets of 10,000 simulations.

On average, one set of 10,000 simulations experienced approximately 7 instances of failure in 50 years among 5 grid cells. The fragility function was applied to each grid cell independently, so many iterations of the design life can result, from simulations with no failures to multiple catastrophic failures (Figure 4.10). With failure, the diameter at breast height may vary both in space and in time. For example, the diameters in year 49 for the average example were 16.9 cm, 4.0 cm, 14.7 cm, 7.9 cm, and 14.7 cm (Figure 4.10a). With only one failure, the vegetation still had the chance to mature (Figure 4.10b), but in the example with multiple catastrophic failures, the diameter was only able to reach a maximum of 6.7 cm (Figure 4.10c). The average case, with 7 failures, could also only affect one side of the mangroves, allowing the other side to reach maturation (Figure 4.10d).

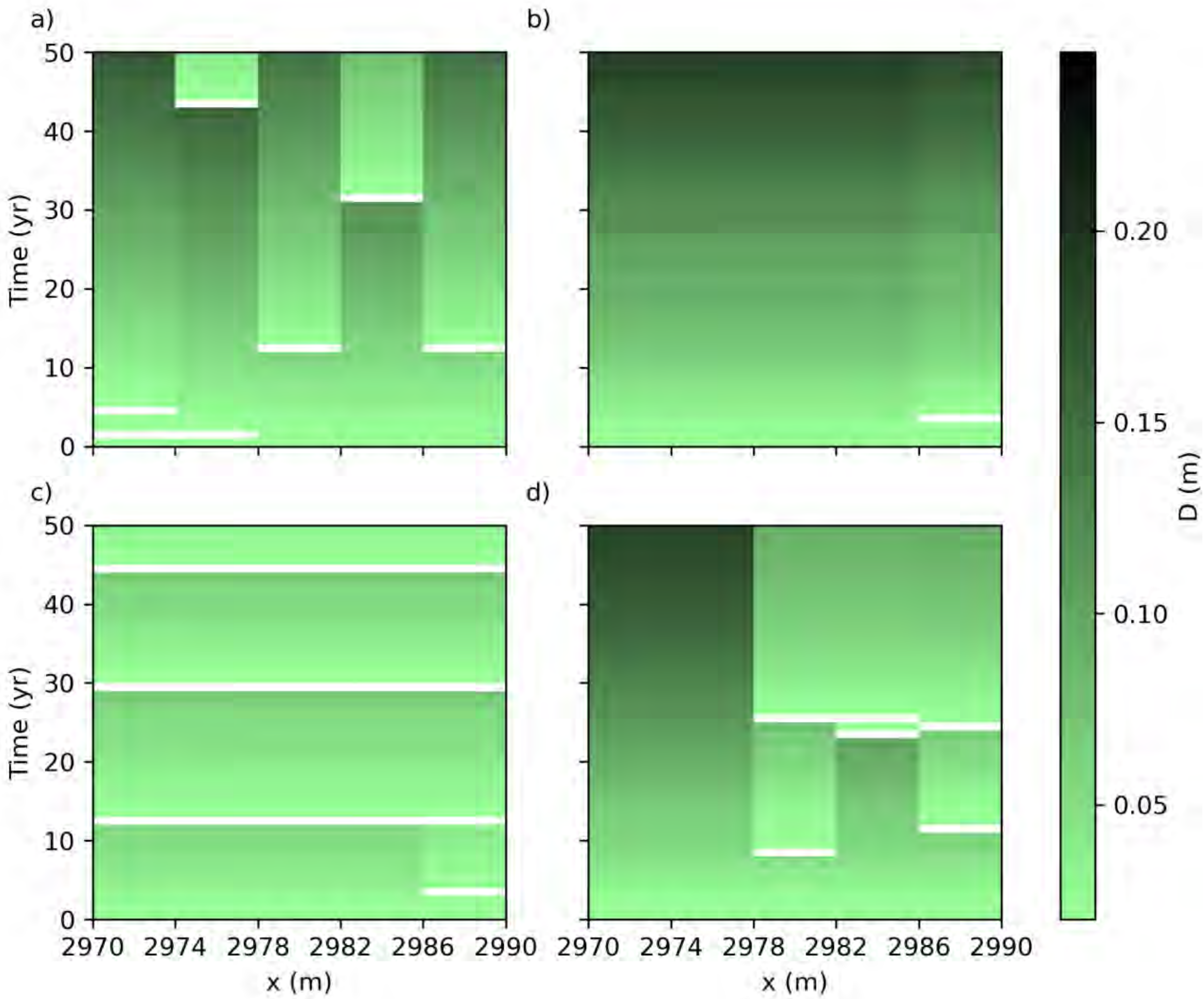

Figure 4.10. Mangrove diameter as a function of time and space for different simulation examples when including Step 4, including cases that show a) the average example with 7 failures spread throughout time and space, b) only one failure, c) multiple catastrophic failures eliminating all of the vegetation, and d) failures only affecting one side of the vegetation. White spaces indicate that structural failure of vegetation occurred in that year and grid cell.

4.2. Model Verification

4.2.1. Allometric Relations

The outputs verified that the model was responding as expected to variations in parameters. Increasing stem density, drag coefficient, and projected area per unit height should result in a smaller value of expected overtopping and probability of failure in any given year, as in Equation (2.3). This result was seen across all parameters tested; for example, increasing the value of stem density led to smaller expected overtopping and probability of failure, all else constant (Figure 4.11). Of the five variables tested, the tested ranges of the height of the trees and height of the roots had the least impact on the performance variables. The other figures are in Appendix D.

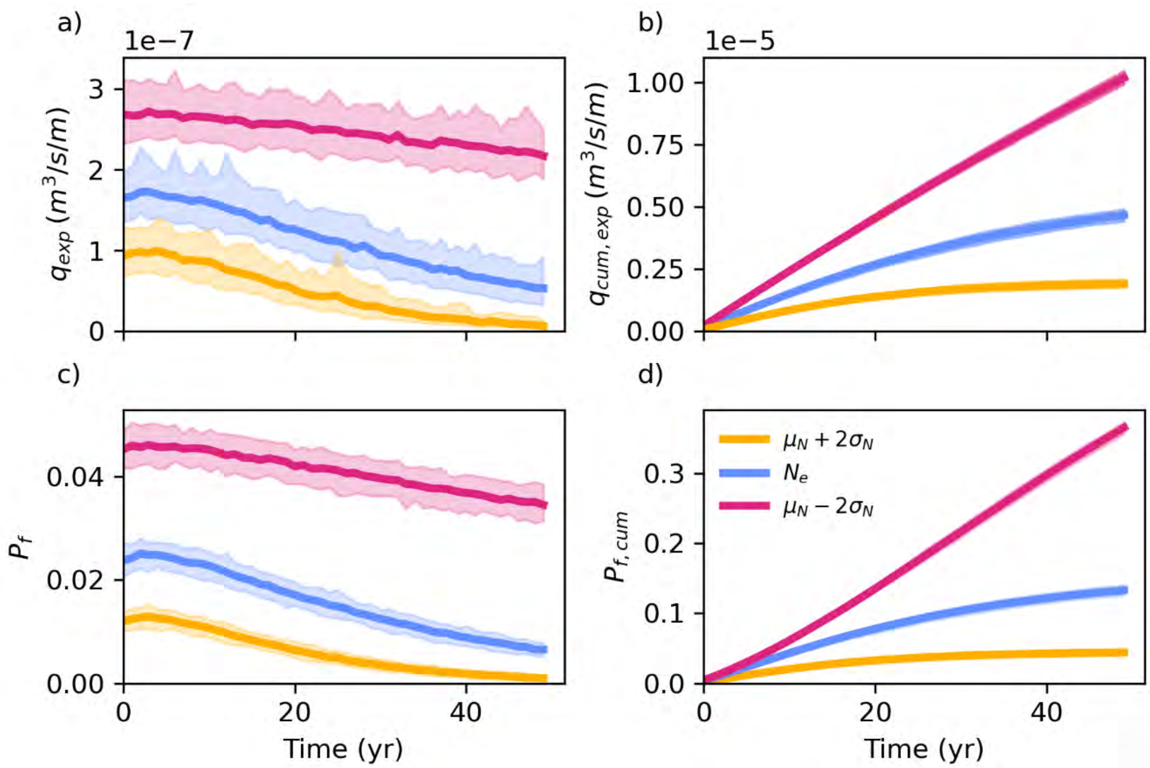

Figure 4.11. Expected performance of the mangrove system for each year of the design life for three stem density relations, with a) the expected value of overtopping, b) the expected cumulative overtopping, c) the probability of failure due to overtopping, and d) the probability of failure due to cumulative overtopping with 95% confidence intervals.

4.2.2. Uncertainty in Parameters

Changing the bias and deviation coefficient for each of the hydrodynamic parameters changed the associated encounter probability of failure (Figure 4.12). As the bias increased for the same deviation coefficient, P_{Ef} increased for each of the parameters. For the significant wave height and transmitted wave height, P_{Ef} increased as the deviation coefficient increased for constant values of the bias. The results contained a larger spread for $\gamma_X = 0$ than $\gamma_X = 0.4$, and the increase in P_{Ef} was larger for $\alpha_X = -0.1$ than $\alpha_X = 0.1$ (Figure 4.12a). The increase in P_{Ef} for each bias value was larger for the transmitted wave height than the significant wave height (Figure 4.12d). For peak period, there was a larger spread in P_{Ef} for $\gamma_X = 0$ than $\gamma_X = 0.4$. For a bias of -0.1, P_{Ef} increased as the deviation coefficient increased, but P_{Ef} decreased as γ_X increased for α_X

= 0.1 (Figure 4.12b). Both the surge and overtopping uncertainty parameters had less of an impact on P_{Ef} than the other hydrodynamic parameters. For surge, P_{Ef} ranged between 69.2% and 73.5% (Figure 4.12c), and for overtopping, it was between 67.6% and 73.7% (Figure 4.12e). Furthermore, these values only changed on the order of 0.1% for different values of deviation coefficient.

The results from changing the bias and deviation coefficient were consistent with the results from Section 4.2.1 (Figure 4.13). As the bias increased, P_{Ef} decreased for stem density, drag coefficient, and projected area of the roots (Figure 4.13a,Figure 4.13b, and Figure 4.13c). As the deviation coefficients increased for constant values of bias, P_{Ef} remained essentially constant; there was a slight increase in P_{Ef}, but this increase was within 2% for each. The differences were much less notable for the height of the roots and height of the trees (Figure 4.13d and 4.13e). For the height of the roots, P_{Ef} increased slightly as the bias increased. The encounter probability of failure only changed when the highest values of deviation coefficient were used. For γ = 0.4, P_{Ef} ranged from 72.5% with α_X = -0.1 and 71.7% with α_X = 0.1. However, the changes for H_R and H_T were all under 1%.

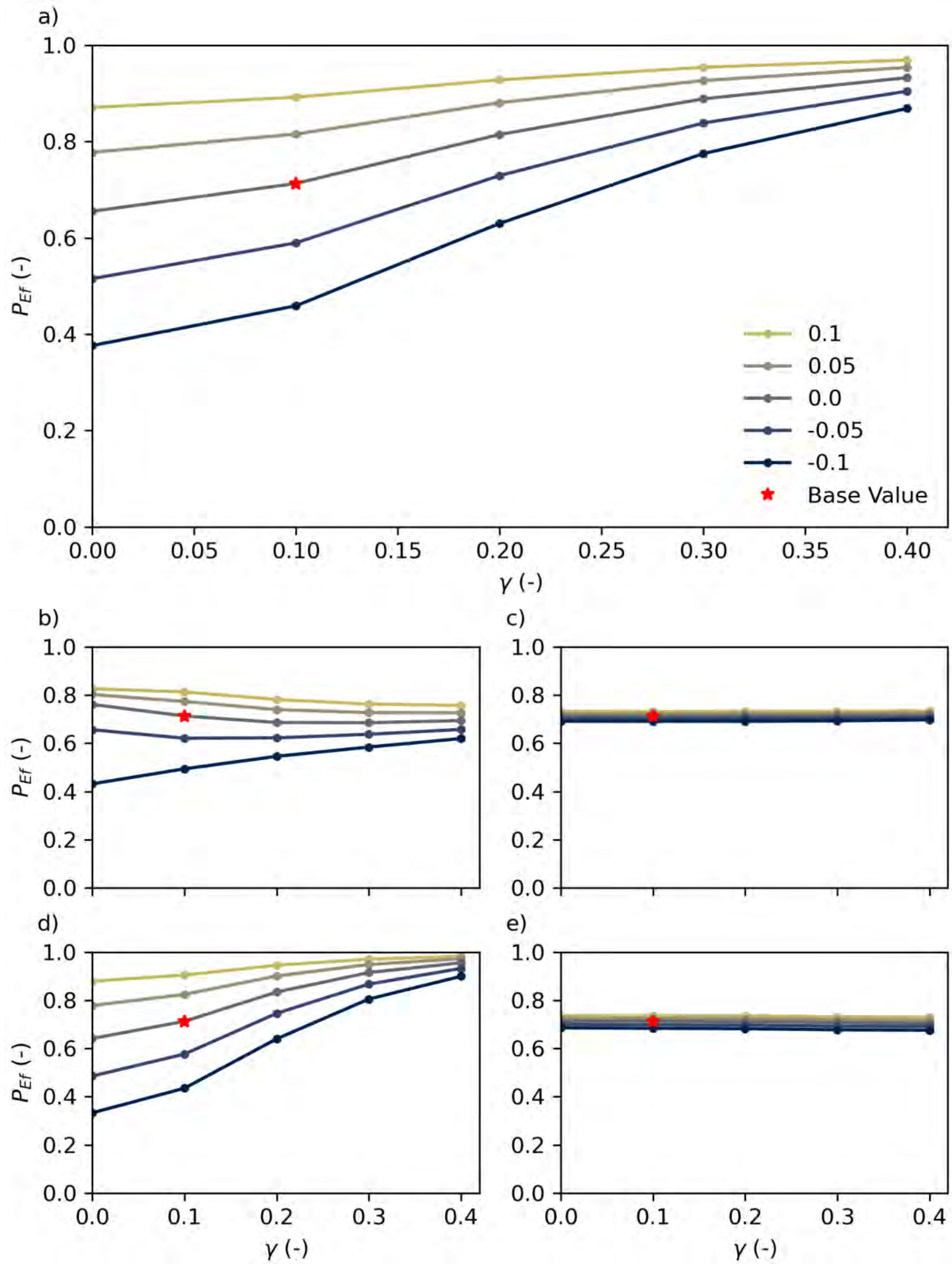

Figure 4.12. Encounter probability of failure as a function of deviation coefficient for multiple bias values for a) significant wave height, b) peak period, c) surge, d) transmitted wave height, and e) overtopping.

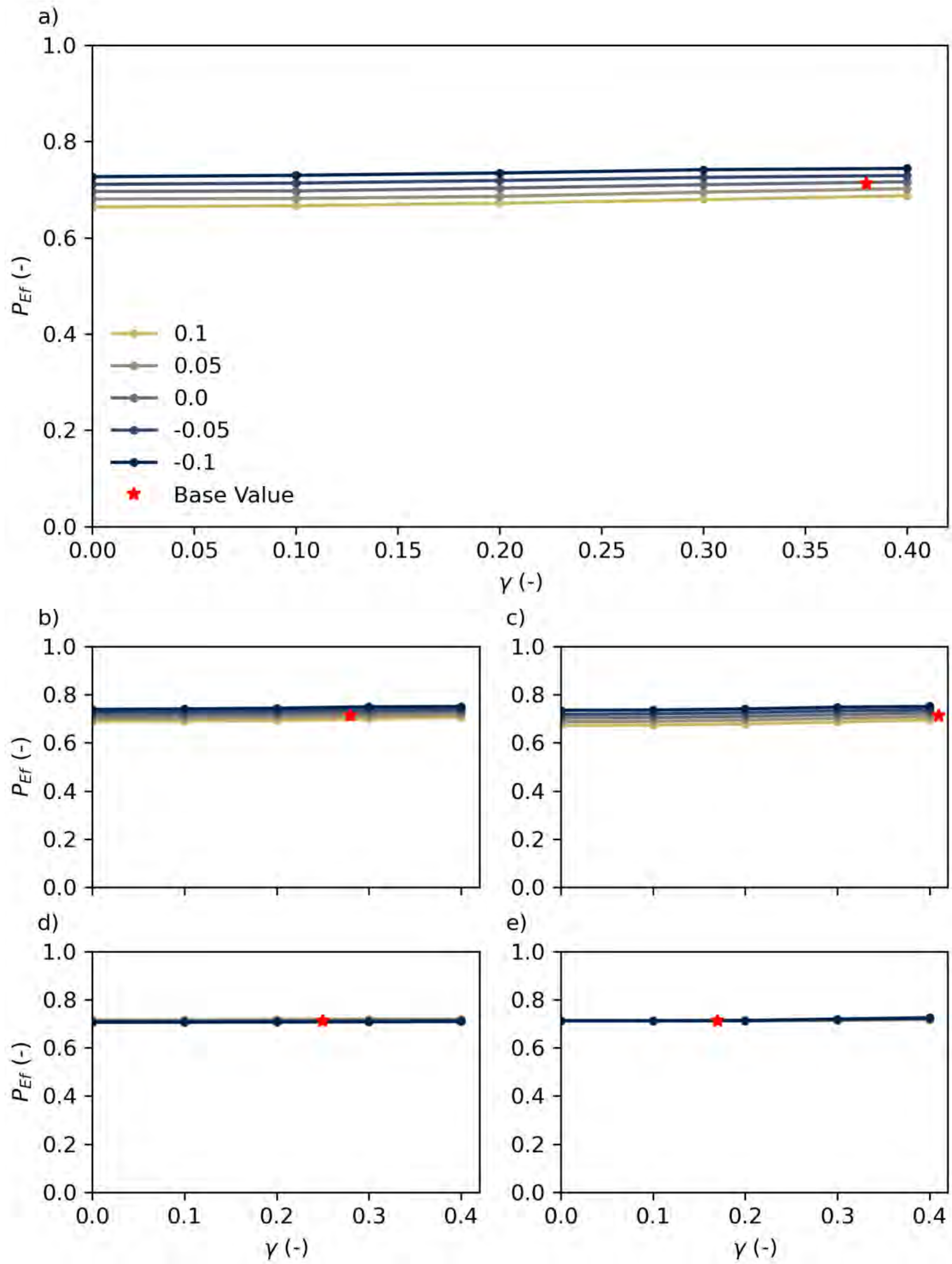

Figure 4.13. Encounter probability of failure as a function of deviation coefficient for multiple bias values for a) drag coefficient, b) projected area of the roots, c) stem density, d) height of the roots, and e) height of the trees.

4.2.3. <u>During-Storm Failure of Vegetation</u>

Changing the median value of the fragility function changed the performance variables (Figure 4.14). When the median decreased, more failure resulted and the probability of failure and expected overtopping increased. When θ_f = 20 m/s, the probability of failure was almost constant throughout the design life, ranging from 0.040 to 0.043 (Figure 4.14c). When θ_f = 24 m/s, there was a larger decrease in the probability of failure and expected overtopping than for the other two cases. The encounter probabilities were 87.9%, 81.7%, and 76.3% for θ_f values of 20 m/s, 22 m/s, and 24 m/s, respectively.

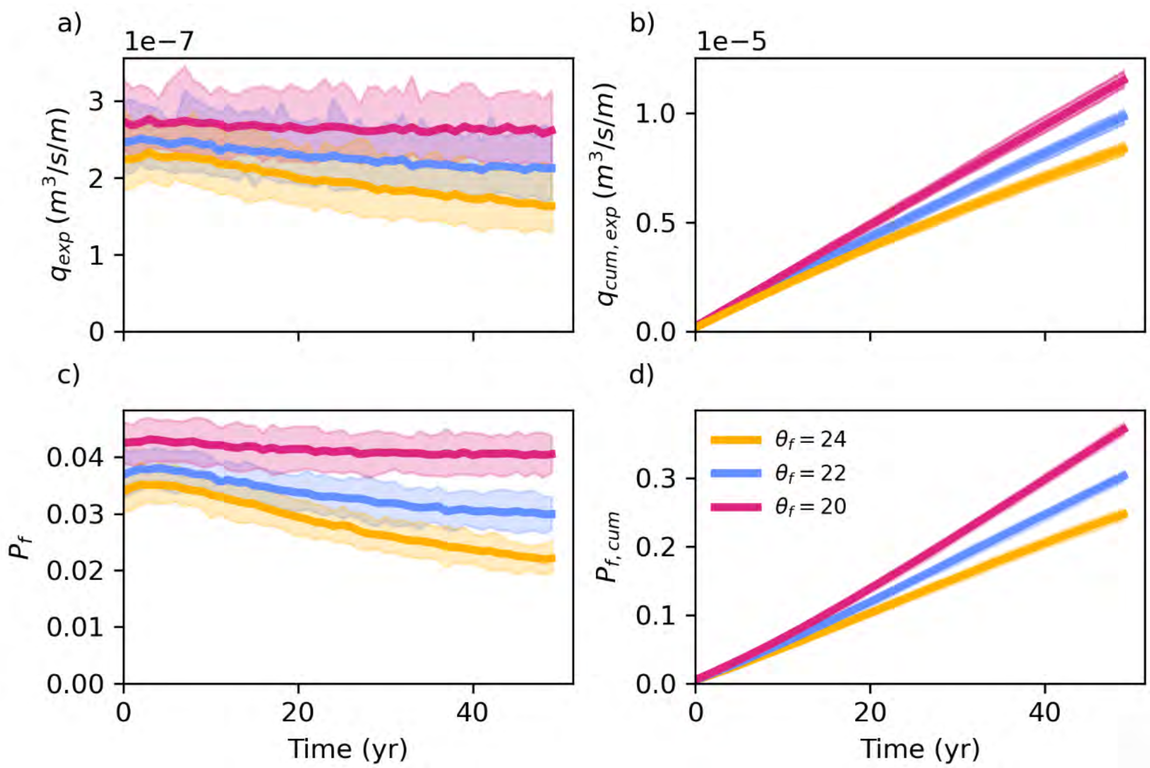

Figure 4.14. Expected performance of the mangrove system for each year of the design life for three median values of the fragility function, with a) the expected value of overtopping, b) the expected cumulative overtopping, c) the probability of failure due to overtopping, and d) the probability of failure due to cumulative overtopping with 95% confidence intervals.

The tested logarithmic standard deviations of the fragility function did not have the same level of impact on the performance variables as the tested median values did (Figure 4.15). The smallest β_f had a slightly lower probability of failure and expected overtopping because the value of the fragility function was smaller for the tested wind speeds.

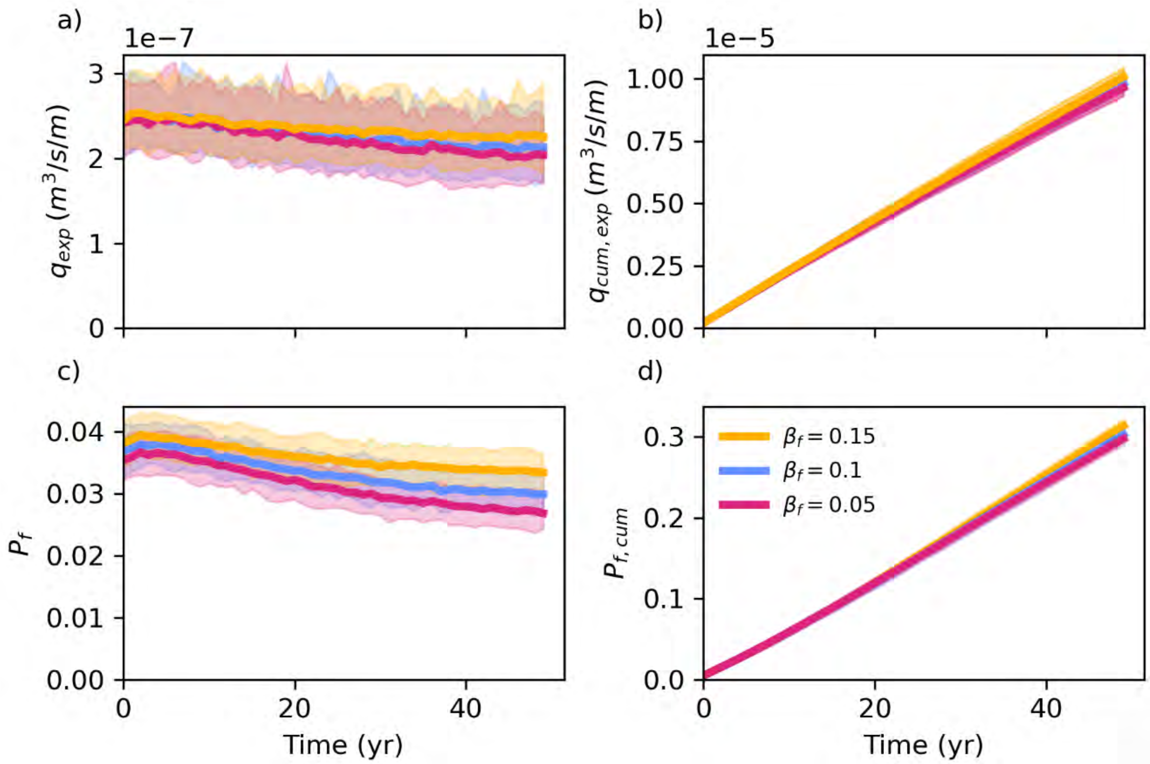

Figure 4.15. Expected performance of the mangrove system for each year of the design life for three logarithmic standard deviations of the fragility function, with a) the expected value of overtopping, b) the expected cumulative overtopping, c) the probability of failure due to overtopping, and d) the probability of failure due to cumulative overtopping with 95% confidence intervals.

5. Discussion

5.1. Expected Performance of Engineering Designs

5.1.1. Effects of Mangroves on Performance Variables

The hybrid system of the mangroves and revetment performed better than the configuration without mangroves. All performance metrics, including the expected overtopping, expected cumulative overtopping, and respective probabilities of failure were reduced in magnitude in comparison to the case with no mangroves. The improved performance in the model reflected the expectations of better performance from the literature (*e.g.,* Tomiczek et al. 2020).

The shape of the probability of failure and expected overtopping curves demonstrated that these performance metrics could not be examined at just one point in time, but that the entire design life needed to be considered. The maximum probability of failure for the 20 m mangrove forest came at year 3, while the minimum occurred at the end of the design life, year 49 (Figure 4.3). The shape of the probability of failure curve reflected the values of the allometric relations. The vegetation parameters were the cause of the changes in the average wave height decay coefficient because the hydrodynamic parameters were stationary. Importantly, the wave height decay coefficients produced from the model (Figure 4.4) were similar to the observed range of wave height decay coefficients from a full-scale experiment (Kelty et al. 2022). Decreases in the drag coefficient and stem density over time were offset by increases in the projected area per unit height (Figure 4.4). The steady improvement in the performance after year 3 contrasted with another study considering performance in time, which found that year 5 had the best performance, year 25 had the worst, and year 35, the final year of the design life, was in between (Maza et al. 2021). The differences may be because Maza et al. (2021) used an empirical wave height attenuation relation based on the submerged volume fraction and utilized different allometric relations.

The vegetation parameters generally fell within values observed in field and lab studies. For example, recommendations for initial stem densities in the literature have varied, with the Asian Development Bank (2018) recommending 5 No./m^2 for propagules, and Teutli-Hernández et al. (2021) recommending a spacing between 1 and 1.5 m. The mean value in the simulation fell within this range. For implementation of this methodology into engineering practice, the allometric relations may need to be modified to reflect local planting recommendations and engineering specifications. The projected area was extrapolated for this study in the absence of data, so more investigation is needed to determine projected areas for mangroves in Southern Florida and mangroves with larger diameters. When implementing this methodology for an engineering project, all allometric relations should be site and species-specific. However, not all data was available for the implementation, so multiple data sources were combined for the allometric relations.

5.1.2. Alternative Designs

The probability of failure curves were different for the two initial mangrove conditions. When starting from propagules, initial diameter was smaller, but the growth rate was larger. The smaller initial diameter led to higher drag coefficients and stem densities in year 0, leading to the observed smaller probability of failure. At the end of the design life, the increased diameter growth rate led to higher projected areas, causing a smaller probability of failure in comparison to the 2-year planted case. While the probabilities of failure were smaller at the beginning and end of the design life, the maximum probability of failure remained the same. Engineers that would like the maximum probability of failure to occur earlier in the design life might use the 2-year planted case, while engineers that prefer better performance at the end of the design life might prefer the propagule case.

Adding additional mangroves drastically improved the performance, reducing the encounter probability of failure from 71.2% with 20 m of mangroves to 7.0% with 160 m of mangroves. The concave-up shape of the curve in Figure 4.7 suggested there may be diminishing returns when adding additional mangroves for this particular case study, and a cost-benefit analysis may be used to identify the ideal length of mangroves to use. This example assumed that *Rhizophora sp.* would be able to grow in all the locations it was applied to, but in reality, elevations and zonation of mangrove species may not allow for these exact configurations to exist. For larger swaths of mangroves, the model should incorporate multiple allometric relations representing different species.

5.1.3. During-Storm Failure of Vegetation

The addition of Step 4 in the model resulted in larger probabilities of failure throughout the design life. The differences were especially pronounced at the end of the design life, as the growth of the projected area per unit height was not as large. The model assumed that there were 2-year old mangroves ready to be replanted after a storm, which may not be feasible. Furthermore, recovery functions may not be the same as the initial allometric relations, as conditions such as debris or sediment may affect growth and vegetation structure (Krauss and Osland 2020; Temmerman et al. 2023). More investigation is required for the implementation of the fragility function, including the grid cell size over which it should be applied and the intensity measure used. For example, vegetation characteristics may be used as a parameter in the fragility function, as smaller mangroves are generally more resistant to storm mortality (Radabaugh et al. 2020; Silveira et al. 2022).

5.2. Model Verification

5.2.1. Allometric Relations

The model responded as expected to changes in the allometric relations. Increases in stem density, drag coefficient, and projected area of the roots all decreased the probability of failure. These three variables had linear relationships with the wave height decay coefficient in Equation (2.3), as A_R had a linear relationship with b_v, indicating the model was working as expected. An increase in the height of the roots resulted in an increase in the probability of failure because H_R had an inverse relationship with b_v for the implementation in Equations (3.19) and (3.21). There was no difference in the performance metrics when increasing or decreasing the height of the trees. This was due to the fact that even when H_T was reduced from the mean by two standard deviations, the trees were submerged only approximately 0.7% of the time, which was not enough to affect the output. Note that the performance variables in the default case in each plot were smaller than in Figure 4.3, because the uncertainty in each of the 10 parameters in Table 3.1 was removed.

5.2.2. Uncertainty

As in Section 5.2.1, changing the uncertainty parameters verified that the model was working as expected. There was generally more variation in encounter probabilities of failure associated with the hydrodynamic variables than the vegetation parameters. However, the study was completed on a 20 m mangrove fringe. If it had been completed over a larger mangrove section, the impact of the different hydrodynamic parameters on the encounter probability would have been larger. The Level III reliability analysis contained the assumption that the error functions were normal distributions; the histograms in Appendix A demonstrated that the error functions may be better approximated with different distributions.

Changing the bias and deviation coefficient for H_s and H_t yielded similar curve shapes. As the bias increased, P_{Ef} increased due to higher waves causing more overtopping events that exceeded the failure threshold. Increasing the deviation coefficient also resulted in higher P_{Ef}, as it created a larger spread of wave heights, leading to more failure events. Decreasing the peak period resulted in steepness-limited breaking for smaller wave heights, reducing the wave heights and therefore the number of overtopping failures. So, when the bias of the peak period was decreased, the encounter probability of failure also decreased. As the deviation coefficient was increased, the encounter probability of failure converged, as the values of T_p converged to similar distributions.

Interestingly, the bias and deviation coefficients for H_s, T_p, and H_t had a larger impact on the encounter probability of failure than the bias and deviation coefficient for overtopping itself. This was because small perturbations in the significant wave height at the revetment used in the overtopping equation, Equation (3.26), resulted in orders of magnitude differences in the overtopping rate, and H_s, T_p, and H_t directly impacted H_{rev}. This contrasted with changing the bias and deviation coefficient for overtopping itself, which resulted in same order of magnitude changes to the encounter probability of failure. For surge and overtopping, the encounter probability of failure remained essentially constant for the tested deviation coefficients. This indicated that the quantification of uncertainty for these two parameters was not as important to the averaged performance metrics.

The changes in the bias and deviation coefficient for stem density, projected area of the roots, and drag coefficient resulted in a range of P_{Ef} values like those seen for overtopping and surge. For the vegetation parameters, the average values dictated the effect on the encounter probability, rather than the spread around the average. As with Section 5.2.1, changing the height of the roots had a smaller impact on the encounter probability of failure than N, C_d, and A_R, due to the projected area per unit height calculation having a larger dependence on A_R rather than H_R. This result did not indicate that the interaction between the height of the roots and mean water depth is not important; another mangrove configuration in shallower water would experience more wave height attenuation. In fact, in all of the bias and deviation coefficient values tested, the height of the roots exceeded the water depth a maximum of 18% of the time (occurring in the case where $\alpha_X = -0.1$ and $\gamma_X = 0.4$). This result indicated that the height of the roots did not need to be known as precisely as the other variables for this case. The encounter probability of failure remained the same for all combinations of the bias and deviation coefficient for the height of the trees, for the same reasons as in 5.2.1.

5.2.3. During-Storm Failure of Vegetation

Differences in the fragility function resulted in different performance metrics. As expected, reducing the median value of the fragility function resulted in more failure, increasing the expected overtopping and probability of failure. For the median value of 20 m/s, the resulting expected overtopping and probability of failure were almost constant, and only slightly decreased from the no mangrove case. The particular β_f values tested did not change the expected performance metrics as much as the median values tested. The smallest value of β_f resulted in the smallest probability of failure, as this value created a steeper fragility function with less failure at the wind speeds examined.

5.3. Model Implementation

5.3.1. Hydrodynamic Assumptions

While the model required hydrodynamic simplifications, some resulted in conservative estimates of the performance variables. For example, it was assumed that no shoaling would occur within the mangroves. This was a conservative assumption for this case study, as the shoaling coefficient was generally less than 1, and incorporating shoaling would have further reduced the wave heights. The addition of tides would have provided an additional independent variable and dependency for the performance variables (Takayama and Ikeda 1993). The addition of tides would have lowered the water depth for some storms, as the water depth used in the model was assumed to be high tide. Tidal variations may be incorporated by establishing them in Step 2 of the methodology. Lower water depths would result in more wave height attenuation, as the projected area per unit height would be larger. Lower water depths would also reduce the orbital velocity, resulting in higher drag coefficients.

Some hydrodynamic simplifications were chosen due to the fidelity of the hydrodynamic model, and not incorporating them would require changing hydrodynamic models. Linear wave theory was assumed for this simplified model even though the waves produced by the fetch-limited algorithm were predominantly Stokes waves. A more accurate representation of the hydrodynamics would have been to use nonlinear wave mechanics. The peak period would not have been constant over the model domain, the drag coefficient would have been different with different orbital velocities, and the wave heights would be modified. The Mendez and Losada (2004) equation would not be strictly valid. The breaking criteria were applied after the uncertainty was applied for H_s, T_p, and H_t. In other words, the breaking criteria were assumed to be accurate. To incorporate these changes, it would be better to increase the fidelity of the hydrodynamics model; an overview of available models can be found in Ostrow et al. (2022). A higher fidelity model could also incorporate the effects of reflection off the vegetation and revetment. The model also assumed a 1D domain with only shore-normal waves. The model could be expanded to a 2D domain so that longshore impacts are included. Furthermore, adding a wind direction would create the need for refraction calculations, which could be added in Step 5 in the model along with shoaling.

The model also assumed that the overtopping equations from existing engineering design standards could be used after the wave height attenuation from the mangroves. More studies are needed to determine if this assumption was valid. There has been evidence that equations for force may be applied from current engineering design guidance without considering vegetation (Mitchell 2021).

5.3.2. Vegetation Assumptions

Limitations in the model should be taken into consideration for design. This iteration of the model implemented a 1D grid, so edge effects were neglected. Furthermore, the assumption of one storm per year meant that any compounding damage from multiple storms in one year was ignored. The model did not include bathymetry changes, which can change the location of mangrove vegetation (*e.g.,* Silveira et al. 2022). Furthermore, the location of the mangroves was assumed to be fixed, and future versions of the model may incorporate the migration of mangroves. The model also approximated the diameter growth rate as a random variable rather than approximating the number of propagules with a random variable and determining the diameter growth rate from environmental conditions, as in the FORMAN ecological model (Chen and Twilley 1998). More work is needed to validate the outputs with ecological models.

Care must be taken for the characterization of the drag coefficient. The calculation of the drag coefficient required specifying a nondimensional number and associated parameters. While Reynolds number was used for this implementation, the Keulegan-Carpenter number, *KC*, has also been frequently reported in drag coefficient studies, and the drag coefficient also has an inverse relationship with *KC* (*e.g.,* Bryant et al. 2022; Chang et al. 2022; Wang et al. 2022). While *Re* has a direct relationship with diameter, therefore leading to larger *Re* values as mangroves age under the same hydrodynamic conditions, *KC* has an inverse relationship with diameter, which would lead to smaller *KC* values over time with the same hydrodynamics. Therefore, if *KC* was used as the nondimensional number, the C_d values would have increased with time. This would have led to higher probability of failure values in the beginning of the design life, and smaller probabilities of failure at the end of the design life compared to using *Re*. More research is needed to characterize the drag coefficient under changing diameters, rather than just changing hydrodynamics.

The relevant length scales and characteristic velocity should be investigated further. Different suggested length scales consider the average projected area (*e.g.,* Maza et al. 2019), an effective diameter considering the number of roots in each tree (Kelty et al. 2022), a hydraulic radius considering the porosity of the roots (Chang et al. 2022), and diameter at breast height, among others. Different length scales have different relations with increasing depth (Kelty 2021), which can affect the value of the drag coefficient used. Furthermore, the inertia coefficient was neglected in this model implementation for conservative design, but it may have a nonnegligible impact on wave height attenuation (Bryant et al. 2022; Chang et al. 2022).

5.4. Climate Change and Other Considerations

Climate change can affect the model through both the hydrodynamics and vegetation conditions. Changes in the hydrodynamics can be incorporated through changing the extreme annual storm distribution and adding sea level rise (*e.g.,* Mase et al. 2013; Suh et al. 2012, 2013) or scaling the performance variables (*e.g.,* Pillai et al. 2019). The vegetation would be expected to respond to changes in hydrodynamic conditions. For example, studies have found that mangroves may accommodate for sea level rise by migrating landwards, and if this retreat is blocked, it would reduce the length over which the vegetation could attenuate waves (Borchert et al. 2018). Extreme events associated with climate change may change mangrove mortality and recovery patterns (Sippo et al. 2018).

Humans can also affect mangrove systems, and these impacts can be incorporated the model. For example, instead of using allometric relations based on existing natural systems, the relations may be modified to match engineering or ecological guidance. Designers may also choose to utilize adaptive management (de Looff et al. 2021). There are multiple ways to incorporate this in the model. For example, any updates to the vegetation conditions can be incorporated in Step 7 of the model. Another option would be to set minimum or maximum values to the allometric relations based on engineering specifications. This performance-based design methodology may also be expanded to other types of NNBF or hybrid systems by replacing the applicable parameters in the model.

6. Conclusion

The objective of this thesis was to expand a Level III performance-based design methodology to emergent vegetation for Natural and Nature-Based Features. That is, this thesis incorporated nonstationary vegetation conditions within a PBD framework. This was accomplished through tracking vegetation growth and mortality throughout the design life. Results showed that performance did not remain constant over the design life and depended on the size of the mangroves. The performance improved when more mangroves were added to the model. The model can also be used to evaluate different mangrove restoration conditions. Adding mangrove mortality worsened the performance metrics in comparison to the case with no mortality, but the system still performed better than without mangroves. The implementation of the methodology was verified, showing that the model responded in an expected way when certain parameters were changed. Changing the value of the bias coefficient did not result in notable differences in the encounter probability of failure, other than those for the significant wave height, peak period, and transmitted wave height, indicating that obtaining the proper equations was generally more important than characterizing the uncertainty.

More work is needed to validate and complete the next version of the model. In the next iteration, based on the validation and more data, the implementation of mangrove growth should be revisited. The next version should also incorporate more refined estimations of mortality, both during-storm and delayed. Fragility functions based on data could be incorporated. Validation should also reveal the consequences of the model assumptions and may result in changes to the model. For example, the model may be run for more than one storm per year or could incorporate an extra probability term for multiple storms in one year.

7. Nomenclature

A	shape parameter of the Gumbel distribution for the wind speed at 10 m
A_R	projected area of the roots normal to the horizontal velocity of each vegetation stem (m^2)
a_1	regression parameter for projected area of the roots
a_2	regression parameter for projected area of the roots
ah	submerged vegetation height (m)
B	location parameter of the Gumbel distribution for the wind speed at 10 m
b_v	projected area per unit height normal to the horizontal orbital velocity of each vegetation stem (m^2/m)
C_d	depth-averaged form drag coefficient (unitless)
c_1	regression coefficient for the drag coefficient
c_2	regression coefficient for the drag coefficient
c_3	regression coefficient for the drag coefficient
D	diameter at breast height (m)
D_0	diameter at breast height in year 0 of the design life (m)
d	depth of the water in the absence of surge (m)
dD/dt	diameter growth rate, defined as the increase in diameter at breast height per year (m/yr)
dD/dt_{max}	maximum diameter growth rate (m/yr)
F	fetch length (m)
F_D	horizontal drag force imparted by vegetation per unit volume (N/m^3)
g	acceleration due to gravity (m/s^2)
EDP	engineering demand parameter
EDP_{exp}	expected engineering demand parameter
edp	critical value of the engineering demand parameter
H_R	height of the roots, defined as the distance above the ground at which the highest root connects to the stem (m)
H_T	height of the trees, defined as the height of each vegetation stem (m)
H_i	initial wave height (m)
H_{rev}	significant wave height at the revetment (m)

H_s	significant wave height (m)
H_t	transmitted wave height (m)
h	water depth (m)
IM	intensity measure
im	specific value of the intensity measure
k	wavenumber derived from linear wave theory (m^{-1})
M	morphology
m	specific value of the morphology
N	stem density, defined as the number of vegetation stems per unit area (No./m^2)
n_1	regression parameter for stem density
n_2	regression parameter for stem density
n_{set}	number of sets of Monte Carlo simulations
n_{sim}	number of Monte Carlo simulations
P_{Ef}	encounter probability of failure, defined as the probability of at least one failure event occurring over the design life (unitless)
P_f	probability of failure with respect to the engineering demand parameter in each year of the design life (unitless)
$P_{f,cum}$	probability of failure with respect to the cumulative engineering demand parameter in each year of the design life (unitless)
p_1	coefficient determining the proportion of the projected area of the roots that lies below a certain water depth (unitless)
q	overtopping rate per unit width in each year of the design life (m^3/s/m)
q_c	critical overtopping rate per unit width (m^3/s/m)
$q_{cum,c}$	critical value of cumulative overtopping rate per unit width (m^3/s/m)
q_{exp}	expected value of overtopping rate per unit width (m^3/s/m)
$q_{cum,exp}$	Expected value of cumulative overtopping per unit width (m^3/s/m)
R_c	freeboard of the revetment (m)
Re	Reynolds number (unitless)
r_1	regression parameter for the height of the roots
r_2	regression parameter for the height of the roots
S	surge height (m)
T_L	length of the design life (yr)

T_p	peak period (s)
t	time (yr)
t_1	regression parameter for the height of the trees
t_2	regression parameter for the height of the trees
t_3	regression parameter for the height of the trees
U	wind speed at 10 m above the ground (m/s)
U_*	friction velocity (m/s)
u	horizontal orbital velocity (m/s)
X	value of a parameter generated within the PBD model
X_E	calculated a value of a parameter generated within the PBD model from equation at values from experiments
X_M	measured a value of a parameter generated within the PBD model from experiments
X_e	value of a parameter generated within the PBD model generated from the associated equation
x	horizontal coordinate (m)
Z	limit state function
α_X	bias of a value of a parameter generated within the PBD model
β	wave height decay coefficient (m^{-1})
β_f	logarithmic standard deviation of the fragility function
γ_B	parameter for short- and long-crested waves depending on angle of incidence (unitless)
γ_S	parameter for front geometry (unitless)
γ_X	deviation coefficient of a value of a parameter generated within the PBD model
θ_f	median of the fragility function
μ_X	mean of the error function associated with a value of a parameter generated within the PBD model
ρ	fluid density (kg/m^3)
σ_X	standard deviation of the error function associated with a value of a parameter generated within the PBD model

8. References

Aktan, A. E., B. R. Ellingwood, and B. Kehoe. 2007. "Performance-Based Engineering of Constructed Systems." *Journal of Structural Engineering*, 133 (3): 311–323. American Society of Civil Engineers. https://doi.org/10.1061/(ASCE)0733-9445(2007)133:3(311).

Alongi, D. M. 2008. "Mangrove forests: Resilience, protection from tsunamis, and responses to global climate change." *Estuarine, Coastal and Shelf Science*, 76 (1): 1–13. https://doi.org/10.1016/j.ecss.2007.08.024.

Alongi, D. M. 2020. "Global Significance of Mangrove Blue Carbon in Climate Change Mitigation." *Sci*, 2 (3): 67. Multidisciplinary Digital Publishing Institute. https://doi.org/10.3390/sci2030067.

Asian Development Bank. 2018. *Community-Based Mangrove Planting Handbook for Papua New Guinea*. Asian Development Bank.

Berger, U., and H. Hildenbrandt. 2000. "A new approach to spatially explicit modelling of forest dynamics: spacing, ageing and neighbourhood competition of mangrove trees." *Ecological Modelling*, 132 (3): 287–302. https://doi.org/10.1016/S0304-3800(00)00298-2.

van Bijsterveldt, C. E. J., A. O. Debrot, T. J. Bouma, M. B. Maulana, R. Pribadi, J. Schop, F. H. Tonneijck, and B. K. van Wesenbeeck. 2022. "To Plant or Not to Plant: When can Planting Facilitate Mangrove Restoration?" *Frontiers in Environmental Science*, 9.

Borchert, S. M., M. J. Osland, N. M. Enwright, and K. T. Griffith. 2018. "Coastal wetland adaptation to sea level rise: Quantifying potential for landward migration and coastal squeeze." *Journal of Applied Ecology*, 55 (6): 2876–2887. https://doi.org/10.1111/1365-2664.13169.

Bridges, T. S., J. K. King, J. D. Simm, M. W. Beck, G. Collins, Q. Lodder, and R. K. Mohan. 2021. *International Guidelines on Natural and Nature-Based Features for Flood Risk Management*. Report. Engineer Research and Development Center (U.S.).

Bryant, M. A., D. B. Bryant, L. A. Provost, N. R. Hurst, M. McHugh, A. Wargula, and T. Tomiczek. 2022. *Wave Attenuation of Coastal Mangroves at a Near-Prototype Scale*. 126. Technical Report. Engineer Research and Development Center (U.S.).

Chang, C.-W., N. Mori, N. Tsuruta, and K. Suzuki. 2019. "Estimation of Wave Force Coefficients on Mangrove Models." *Journal of Japan Society of Civil Engineers, Ser. B2 (Coastal Engineering)*, 75 (2): I_1105-I_1110. https://doi.org/10.2208/kaigan.75.I_1105.

Chang, C.-W., N. Mori, N. Tsuruta, K. Suzuki, and H. Yanagisawa. 2022. "An Experimental Study of Mangrove-Induced Resistance on Water Waves Considering the Impacts of Typical Rhizophora Roots." *Journal of Geophysical Research: Oceans*, 127 (6): e2022JC018653. https://doi.org/10.1029/2022JC018653.

Chen, H.-P., and A. M. Alani. 2012. "Reliability and optimised maintenance for sea defences." *Proceedings of the Institution of Civil Engineers - Maritime Engineering*, 165 (2): 51–64. https://doi.org/10.1680/maen.2010.37.

Chen, R., and R. R. Twilley. 1998. "A gap dynamic model of mangrove forest development along gradients of soil salinity and nutrient resources." *Journal of Ecology*, 86 (1): 37–51. https://doi.org/10.1046/j.1365-2745.1998.00233.x.

Cherry, C., B. Dix, S. Asam, B. Webb, and S. Douglass. 2018. *Peer Exchange Summary Report: Nature-Based Solutions for Coastal Highway Resilience*. Washington, DC: Federal Highway Administration.

Cintrón, G., and Y. Schaeffer-Novelli. 1984. "Methods for studying mangrove structure." *The mangrove ecosystem: research methods*, Monographs on oceanographic methodology, S. C. Snedaker and J. G. Snedaker, eds., 251. UNESCO.

Close, S. L., F. Montalto, P. Orton, A. Antoine, D. Peters, H. Jones, A. Parris, and A. Blumberg. 2017. "Achieving sustainability goals for urban coasts in the US Northeast: research needs and challenges." *Local Environment*, 22 (4): 508–522. Routledge. https://doi.org/10.1080/13549839.2016.1233526.

Coops, H., N. Geilen, H. J. Verheij, R. Boeters, and G. van der Velde. 1996. "Interactions between waves, bank erosion and emergent vegetation: an experimental study in a wave tank." *Aquatic Botany*, 53 (3): 187–198. https://doi.org/10.1016/0304-3770(96)01027-3.

Craighead, F. C., and V. C. Gilbert. 1962. "The Effects of Hurricane Donna on the Vegetation of Southern Florida." *Quarterly Journal of the Florida Academy of Sciences*, 25 (1): 1–28.

Dalrymple, R. A., J. T. Kirby, and P. A. Hwang. 1984. "Wave Diffraction Due to Areas of Energy Dissipation." *Journal of Waterway, Port, Coastal, and Ocean Engineering*, 110 (1): 67–79. American Society of Civil Engineers. https://doi.org/10.1061/(ASCE)0733-950X(1984)110:1(67).

Dean, R. G., and R. A. Dalrymple. 1984. *Water Wave Mechanics for Engineers and Scientists*. Advanced Series on Ocean Engineering. Singapore: World Scientific Publishing Co.

Doyle, T. W. 1995. "Wind Damage Effects of Hurricane Andrew on Mangrove Communities Along the Southwest Coast of Florida, USA." *Journal of Coastal Research*, (21): 11.

Franco, C., and L. Franco. 1999. "Overtopping Formulas for Caisson Breakwaters with Nonbreaking 3D Waves." *Journal of Waterway, Port, Coastal, and Ocean Engineering*, 125 (2): 98–108. American Society of Civil Engineers. https://doi.org/10.1061/(ASCE)0733-950X(1999)125:2(98).

Gedan, K. B., M. L. Kirwan, E. Wolanski, E. B. Barbier, and B. R. Silliman. 2011. "The present and future role of coastal wetland vegetation in protecting shorelines: answering recent challenges to the paradigm." *Climatic Change*, 106 (1): 7–29. https://doi.org/10.1007/s10584-010-0003-7.

Gijón Mancheño, A., V. Vuik, B. K. van Wesenbeeck, S. N. (Bas) Jonkman, R. Moll, S. Kazi, I. M. Urrutia Duarte, and M. V. Ledden. 2022. *Wave Reduction by Mangroves during Cyclones in Bangladesh: Implementing Nature-Based Solutions for Coastal Resilience*. Policy Research working paper. Washington, DC: World Bank Group.

Goda, Y. 2010. *Random Seas and Design of Maritime Structures*. Advanced Series on Ocean Engineering. World Scientific.

Harper, B. A., J. D. Kepert, and J. D. Ginger. 2010. *Guidelines for Converting Between Various Wind Averaging Periods in Tropical Cyclone Conditions*. Geneva, Switzerland: World Meterological Organization.

Harris, C. R., K. J. Millman, S. J. van der Walt, R. Gommers, P. Virtanen, D. Cournapeau, E. Wieser, J. Taylor, S. Berg, N. J. Smith, R. Kern, M. Picus, S. Hoyer, M. H. van Kerkwijk, M. Brett, A. Haldane, J. F. del Río, M. Wiebe, P. Peterson, P. Gérard-Marchant, K. Sheppard, T. Reddy, W. Weckesser, H. Abbasi, C. Gohlke, and T. E. Oliphant. 2020. "Array programming with NumPy." *Nature*, 585 (7825): 357–362. Nature Publishing Group. https://doi.org/10.1038/s41586-020-2649-2.

Hong, S. Y., K.-D. Suh, and H.-M. Kweon. 2004. "Calculation of Expected Sliding Distance of Breakwater Caisson Considering Variability in Wave Direction." *Coastal Engineering Journal*, 46 (1): 119–140. Taylor & Francis. https://doi.org/10.1142/S0578563404000987.

Hurff, K. 2016. "A Contemporary Approach to a Classic Model: Exploring the Influence of Local Interactions and Disturbance on Mangrove Forest Dynamics with a Spatially-Explicit Version of FORMAN." Master of Science. Louisiana State University and Agricultural and Mechanical College.

Jimenez, J. A., A. E. Lugo, and G. Cintron. 1985. "Tree Mortality in Mangrove Forests." *Biotropica*, 17 (3): 177–185. [Association for Tropical Biology and Conservation, Wiley]. https://doi.org/10.2307/2388214.

Kelty, K. 2021. "Prototype-Scale Physical Model Study of Wave Attenuation by an Idealized Mangrove Forest of Moderate Cross-shore Width." MS Thesis. Corvallis, OR: Oregon State University.

Kelty, K., T. Tomiczek, D. T. Cox, P. Lomonaco, and W. Mitchell. 2022. "Prototype-Scale Physical Model of Wave Attenuation Through a Mangrove Forest of Moderate Cross-Shore Thickness: LiDAR-Based Characterization and Reynolds Scaling for Engineering With Nature." *Frontiers in Marine Science*, 8. https://doi.org/10.3389/fmars.2021.780946.

Krauss, K. W., and M. J. Osland. 2020. "Tropical cyclones and the organization of mangrove forests: a review." *Annals of Botany*, 125 (2): 213–234. https://doi.org/10.1093/aob/mcz161.

Lawrimore, J. H., R. Ray, S. Applequist, B. Korzeniewski, and M. J. Menne. 2016. "Global Summary of the Year (GSOY), Version 1." NOAA National Centers for Environmental Information.

Liénard, J., K. Lynn, N. Strigul, B. K. Norris, D. Gatziolis, J. C. Mullarney, K. Bryan R., and S. M. Henderson. 2016. "Efficient three-dimensional reconstruction of aquatic vegetation geometry: Estimating morphological parameters influencing hydrodynamic drag." *Estuarine, Coastal and Shelf Science*, 178: 77–85. https://doi.org/10.1016/j.ecss.2016.05.011.

de Looff, H., T. Welp, N. Snider, and R. Wilmink. 2021. "Chapter 7: Adaptive Management." *International Guidelines on Natural and Nature-Based Features for Flood Risk Management*, T. S. Bridges, J. K. King, J. D. Simm, M. W. Beck, G. Collins, Q. Lodder, and R. K. Mohan, eds. Vicksburg, MS: U.S. Army Engineer Research and Development Center.

Lugo, A. E. 1980. "Mangrove Ecosystems: Successional or Steady State?" *Biotropica*, 12 (2): 65–72. [Association for Tropical Biology and Conservation, Wiley]. https://doi.org/10.2307/2388158.

Mase, H., D. Tsujio, T. Yasuda, and N. Mori. 2013. "Stability analysis of composite breakwater with wave-dissipating blocks considering increase in sea levels, surges and waves due to climate change." *Ocean Engineering*, Sea Level Rise and Impacts on Engineering Practice, 71: 58–65. https://doi.org/10.1016/j.oceaneng.2012.12.037.

Maza, M., J. L. Lara, and I. J. Losada. 2019. "Experimental analysis of wave attenuation and drag forces in a realistic fringe Rhizophora mangrove forest." *Advances in Water Resources*, 131: 103376. https://doi.org/10.1016/j.advwatres.2019.07.006.

Maza, M., J. L. Lara, and I. J. Losada. 2021. "Predicting the evolution of coastal protection service with mangrove forest age." *Coastal Engineering*, 168: 103922. https://doi.org/10.1016/j.coastaleng.2021.103922.

Mendez, F. J., and I. J. Losada. 2004. "An empirical model to estimate the propagation of random breaking and nonbreaking waves over vegetation fields." *Coastal Engineering*, 51 (2): 103–118. https://doi.org/10.1016/j.coastaleng.2003.11.003.

Menéndez, P., I. J. Losada, S. Torres-Ortega, S. Narayan, and M. W. Beck. 2020. "The Global Flood Protection Benefits of Mangroves." *Sci Rep*, 10 (1): 4404. Nature Publishing Group. https://doi.org/10.1038/s41598-020-61136-6.

Mitchell, W. T. 2021. "Effect of an Idealized Mangrove Forest of Moderate Cross-shore Width on Loads Measured on a Sheltered Structure and Comparison with Predicted Forces." MS Thesis. Corvallis, OR: Oregon State University.

Moehle, J., and G. G. Deierlein. 2004. "A framework methodology for performance-based earthquake engineering." *13th World Conference on Earthquake Engineering*. Vancouver, B.C., Canada.

Mori, N., C.-W. Chang, T. Inoue, Y. Akaji, K. Hinokidani, S. Baba, M. Takagi, S. Mori, H. Koike, M. Miyauchi, R. Suganuma, A. Sabunas, T. Miyashita, and T. Shimura. 2022. "Parameterization of Mangrove Root Structure of Rhizophora stylosa in Coastal Hydrodynamic Model." *Front. Built Environ.*, 7: 782219. https://doi.org/10.3389/fbuil.2021.782219.

Narayan, S., M. W. Beck, B. G. Reguero, I. J. Losada, B. van Wesenbeeck, N. Pontee, J. N. Sanchirico, J. C. Ingram, G.-M. Lange, and K. A. Burks-Copes. 2016. "The Effectiveness, Costs and Coastal Protection Benefits of Natural and Nature-Based Defences." *PLOS ONE*, 11 (5): e0154735. Public Library of Science. https://doi.org/10.1371/journal.pone.0154735.

National Academies of Sciences, Engineering, and Medicine. 2022. "Benefits, Applications, and Opportunities of Natural Infrastructure: Proceedings of a Workshop—in Brief." Washington, DC: The National Academies Press.

National Academy of Sciences. 1977. *Methodology for Calculating Wave Action Effects Associated with Storm Surges*. 29. Washington, DC: National Academy of Sciences.

Novitzky, P. 2010. "Analysis of Mangrove Structure and Latitudinal Relationships on the Gulf Coast of Peninsular Florida." M.A. Thesis. University of South Florida.

Ohira, W., K. Honda, M. Nagai, and A. Ratanasuwan. 2013. "Mangrove stilt root morphology modeling for estimating hydraulic drag in tsunami inundation simulation." *Trees*, 27 (1): 141–148. https://doi.org/10.1007/s00468-012-0782-8.

Ostrow, K., D. T. Cox, G. Guannel, E. L. Biondi, and T. Tomiczek. 2023. "How reliable is emergent vegetation for engineering with nature?" *Coastal Sediments 2023*, 2126–2137. WORLD SCIENTIFIC.

Ostrow, K., G. Guannel, E. L. Biondi, D. T. Cox, and T. Tomiczek. 2022. "State of the practice and engineering framework for using emergent vegetation in coastal infrastructure." *Frontiers in Built Environment*, 8.

Piercy, C. D., N. Pontee, S. Narayan, J. Davis, and T. Meckley. 2021. "Chapter 10: Coastal Wetlands and Tidal Flats." *International Guidelines on Natural and Nature-Based Features for Flood Risk Management*, T. S. Bridges, J. K. King, J. D. Simm, M. W. Beck, G. Collins, Q. Lodder, and R. K. Mohan, eds. Vicksburg, MS: U.S. Army Engineer Research and Development Center.

Pillai, K., C. Lemckert, A. Etemad-Shahidi, L. Cappietti, and S. Sigurdarson. 2019. "Effect of Sea Level Rise on the Wave Overtopping Rate at Berm Breakwater." *Journal of Waterway, Port, Coastal, and Ocean Engineering*, 145 (5): 04019019. American Society of Civil Engineers. https://doi.org/10.1061/(ASCE)WW.1943-5460.0000522.

Pullen, T., N. W. H. Allsop, T. Bruce, A. Kortenhaus, H. Schüttrumpf, and J. W. van der Meer. 2007. *EurOtop wave overtopping of sea defences and related structures: assessment manual*.

Radabaugh, K. R., R. P. Moyer, A. R. Chappel, E. E. Dontis, C. E. Russo, K. M. Joyse, M. W. Bownik, A. H. Goeckner, and N. S. Khan. 2020. "Mangrove Damage, Delayed Mortality, and Early Recovery Following Hurricane Irma at Two Landfall Sites in Southwest Florida, USA." *Estuaries and Coasts*, 43 (5): 1104–1118. https://doi.org/10.1007/s12237-019-00564-8.

Rohatgi, A. 2022. "WebPlotDigitizer." Accessed July 2, 2023. https://automeris.io/WebPlotDigitizer.

Schott, T., C. Landsea, G. Hafele, J. Lorens, A. Taylor, H. Thurm, B. Ward, M. Willis, and W. Zaleski. 2012. "The Saffir-Simpson Hurricane Wind Scale." National Oceanic and Atmospheric Administration.

Seabold, S., and J. Perktold. 2010. "Statsmodels: Econometric and Statistical Modeling with Python." *Proceedings of the 9th Python in Science Conference*, 92–96. https://doi.org/10.25080/Majora-92bf1922-011.

Shimosako, K., and S. Takahashi. 1998. "Reliability Design Method of Composite Breakwaters Using Expected Sliding Distance." *Rept. Port and Harbor Res. Inst.*, 37 (3): 3–30.

Silveira, J. A. H., C. T. Hernandez, F. S. Fajardo, R. Braun, J. Bowman, L. Geselbracht, M. Musgrove, M. Rogers, J. Schmidt, P. J. R. Toral, J. A. C. Cabrera, and L. G. Cano. 2022. *Hurricane Damages to Mangrove Forests and Post-Storm Restoration Techniques and Costs*. Arlington, VA: The Nature Conservancy.

Silvester, R. 1970. "Computation of Storm Surge." *Coastal Engineering Proceedings*, (12): 121–121. https://doi.org/10.9753/icce.v12.121.

Simarro, G., and A. Orfila. 2013. "Improved explicit approximation of linear dispersion relationship for gravity waves: Another discussion." *Coastal Engineering*, 80: 15. https://doi.org/10.1016/j.coastaleng.2013.05.003.

Sippo, J. Z., C. E. Lovelock, I. R. Santos, C. J. Sanders, and D. T. Maher. 2018. "Mangrove mortality in a changing climate: An overview." *Estuarine, Coastal and Shelf Science*, 215: 241–249. https://doi.org/10.1016/j.ecss.2018.10.011.

Snedaker, S. C. 1982. "Mangrove species zonation: why?" *Contributions to the ecology of halophytes*, Tasks for vegetation science, D. N. Sen and K. S. Rajpurohit, eds., 111–125. Dordrecht: Springer Netherlands.

Suh, K.-D., S.-W. Kim, S. Kim, and S. Cheon. 2013. "Effects of climate change on stability of caisson breakwaters in different water depths." *Ocean Engineering*, Sea Level Rise and Impacts on Engineering Practice, 71: 103–112. https://doi.org/10.1016/j.oceaneng.2013.02.017.

Suh, K.-D., S.-W. Kim, N. Mori, and H. Mase. 2012. "Effect of Climate Change on Performance-Based Design of Caisson Breakwaters." *Journal of Waterway, Port,* *Coastal, and Ocean Engineering*, 138 (3): 215–225. American Society of Civil Engineers. https://doi.org/10.1061/(ASCE)WW.1943-5460.0000126.

Taillardat, P., D. A. Friess, and M. Lupascu. 2018. “Mangrove blue carbon strategies for climate change mitigation are most effective at the national scale.” *Biology Letters*, 14 (10): 20180251. Royal Society. https://doi.org/10.1098/rsbl.2018.0251.

Takahashi, S., K. Shimosako, and K. Kimura. 2001. “Performance design for maritime structures and its application to vertical breakwaters-Caisson sliding and deformation-based reliability design.” *Proceedings of International Workshop on Advanced Design of Maritime Structures in the 21st Century*, Y. Goda and S. Takahashi, eds., 63–73. Yokosuka, Japan: Port and Harbour Tech. Res. Inst.

Takayama, T., and N. Ikeda. 1993. *Estimation of Sliding Failure Probability of Present Breakwaters for Probabilistic Design*. Port and Airport Research Institute.

Taylor, M. D. M. R. B., J. L. Rangel-Salazar, and B. C. Hernández. 2013. “Resilience in a Mexican Pacific Mangrove after Hurricanes: Implications for Conservation Restoration.” *Journal of Environmental Protection*, 4 (12): 1383–1391. Scientific Research Publishing. https://doi.org/10.4236/jep.2013.412159.

Temmerman, S., E. M. Horstman, K. W. Krauss, J. C. Mullarney, I. Pelckmans, and K. Schoutens. 2023. “Marshes and Mangroves as Nature-Based Coastal Storm Buffers.” *Annual Review of Marine Science*, 15 (1): null. https://doi.org/10.1146/annurev-marine-040422-092951.

Teutli-Hernández, C., J. A. Herrera-Silveira, D. J. Cisneros-de la Cruz, D. Arceo-Carranza, A. Canul-Cabrera, P. J. Robles-Toral, O. J. Pérez-Martínez, D. Sierra-Oramas, K. Zenteno, H. G. Us-Balam, E. Pech-Poot, X. Chiappa-Carra, and F. A. Comín. 2021. *Manual for the ecological restoration of mangroves in the Mesoamerican Reef System and the Wider Caribbean*. Guatemala City, Guatemala: Integrated Ridge-to-Reef Management of the Mesoamerican Reef Ecoregion Project - MAR2R, UNEP-Cartagena Convention, Mesoamerican Reef Fund.

Tomiczek, T., K. O’Donnell, K. Furman, B. Webbmartin, and S. Scyphers. 2020. “Rapid Damage Assessments of Shorelines and Structures in the Florida Keys after Hurricane Irma.” *Natural Hazards Review*, 21 (1): 05019006. American Society of Civil Engineers. https://doi.org/10.1061/(ASCE)NH.1527-6996.0000349.

Tomiczek, T., A. Wargula, N. R. Hurst, D. B. Bryant, and L. A. Provost. 2021. *Engineering With Nature: The Role of Mangroves in Coastal Protection*. Report. Environmental Laboratory (U.S.).

Twilley, R. R., V. H. Rivera-Monroy, R. Chen, and L. Botero. 1999. “Adapting an Ecological Mangrove Model to Simulate Trajectories in Restoration Ecology.” *Marine Pollution Bulletin*, 37 (8): 404–419. https://doi.org/10.1016/S0025-326X(99)00137-X.

USACE. 2002. *Coastal Engineering Manual*. Washington, DC: USACE.

Virtanen, P., R. Gommers, T. E. Oliphant, M. Haberland, T. Reddy, D. Cournapeau, E. Burovski, P. Peterson, W. Weckesser, J. Bright, S. J. van der Walt, M. Brett, J. Wilson, K. J. Millman, N. Mayorov, A. R. J. Nelson, E. Jones, R. Kern, E. Larson, C. J. Carey, İ. Polat, Y. Feng, E. W. Moore, J. VanderPlas, D. Laxalde, J. Perktold, R. Cimrman, I. Henriksen, E. A. Quintero, C. R. Harris, A. M. Archibald, A. H. Ribeiro, F. Pedregosa, and P. van Mulbregt. 2020. “SciPy 1.0: fundamental algorithms for scientific computing in Python.” *Nat Methods*, 17 (3): 261–272. Nature Publishing Group. https://doi.org/10.1038/s41592-019-0686-2.

Vo, Q. T., C. Kuenzer, Q. M. Vo, F. Moder, and N. Oppelt. 2012. “Review of valuation methods for mangrove ecosystem services.” *Ecological Indicators*, 23: 431–446. https://doi.org/10.1016/j.ecolind.2012.04.022.

Wang, Y., Z. Yin, and Y. Liu. 2022. “Experimental investigation of wave attenuation and bulk drag coefficient in mangrove forest with complex root morphology.” *Applied Ocean Research*, 118: 102974. https://doi.org/10.1016/j.apor.2021.102974.

Ward, G. A., T. J. Smith, K. R. T. Whelan, and T. W. Doyle. 2006. “Regional processes in mangrove ecosystems: spatial scaling relationships, biomass, and turnover rates following catastrophic disturbance.” *Hydrobiologia*, 569 (1): 517–527. https://doi.org/10.1007/s10750-006-0153-9.

Xiong, Y., R. Cakir, S. M. Phan, A. Ola, K. W. Krauss, and C. E. Lovelock. 2019. “Global patterns of tree stem growth and stand aboveground wood production in mangrove forests.” *Forest Ecology and Management*, 444: 382–392. https://doi.org/10.1016/j.foreco.2019.04.045.

Yanagisawa, H., S. Koshimura, K. Goto, T. Miyagi, F. Imamura, A. Ruangrassamee, and C. Tanavud. 2009. “The reduction effects of mangrove forest on a tsunami based on field surveys at Pakarang Cape, Thailand and numerical analysis.” *Estuarine, Coastal and Shelf Science*, 81 (1): 27–37. https://doi.org/10.1016/j.ecss.2008.10.001.

Yoshikai, M., T. Nakamura, R. Suwa, R. Rollon, and K. Nadaoka. 2021. “Measurement and Modeling of Above-Ground Root Systems as Attributes of Flow and Wave Attenuation Function of Mangroves.” *Mangroves: Ecology, Biodiversity and Management*, R. P. Rastogi, M. Phulwaria, and D. K. Gupta, eds., 279–303. Singapore: Springer.

Zhang, X., V. P. Chua, and H.-F. Cheong. 2015. “Hydrodynamics in mangrove prop roots and their physical properties.” *Journal of Hydro-environment Research*, Special Issue on Environmental Hydraulics, 9 (2): 281–294. https://doi.org/10.1016/j.jher.2014.07.010.

APPENDICES

Appendix A. Bias and Deviation Coefficient Estimates

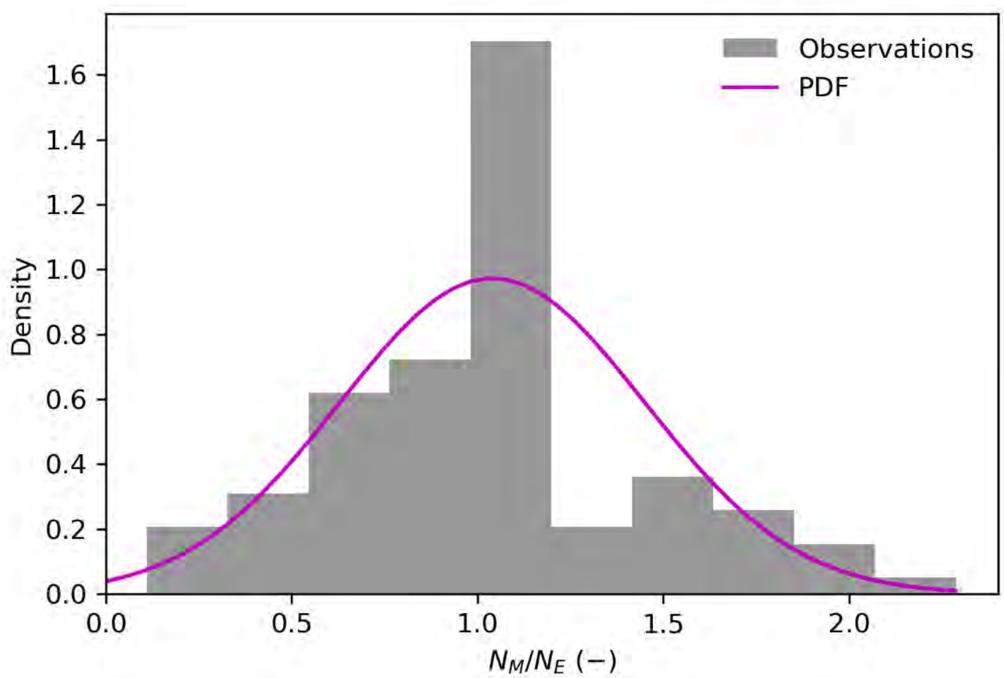

Figure A.1. Density histogram of the ratio of observations of stem density to the calculated value from the regression.

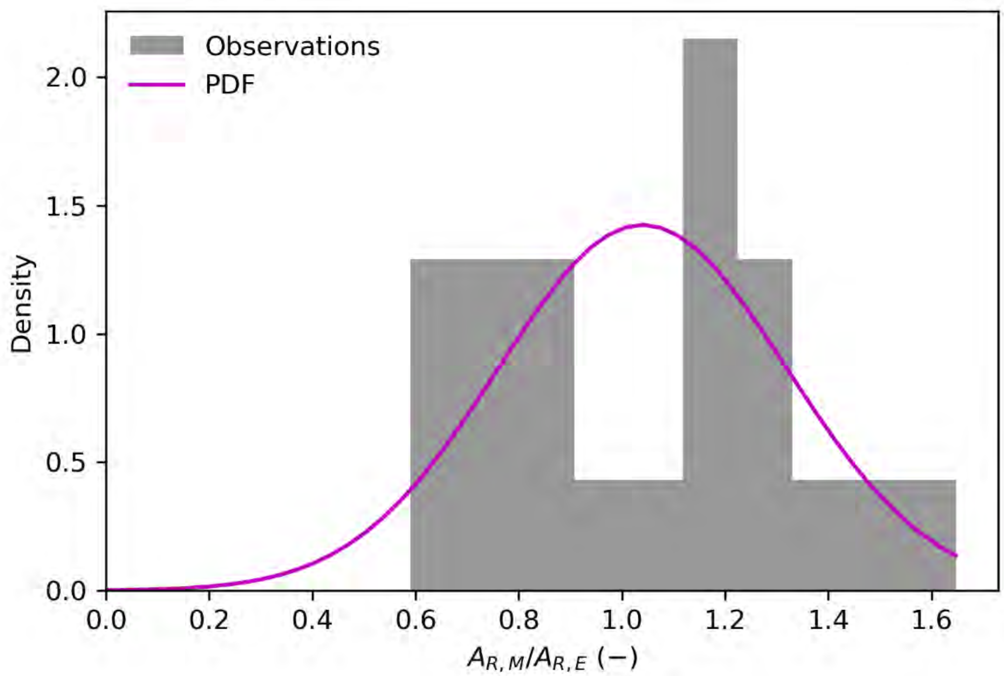

Figure A.2. Density histogram of the ratio of observations of projected area of the roots to the calculated value from the regression.

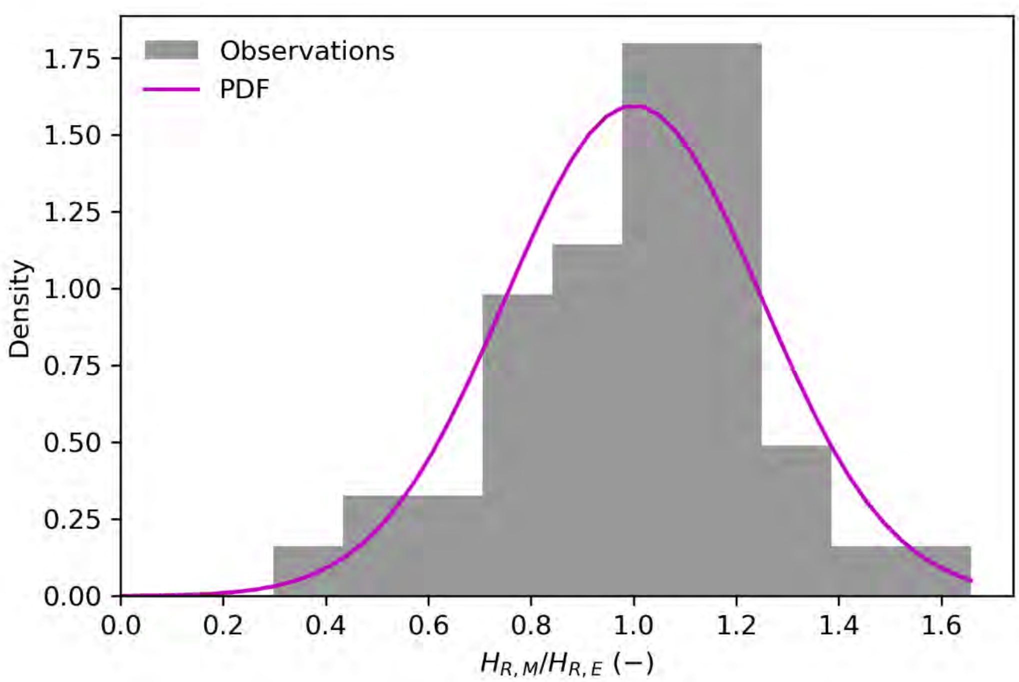

Figure A.3. Density histogram of the ratio of observations of height of the roots to the calculated value from the regression.

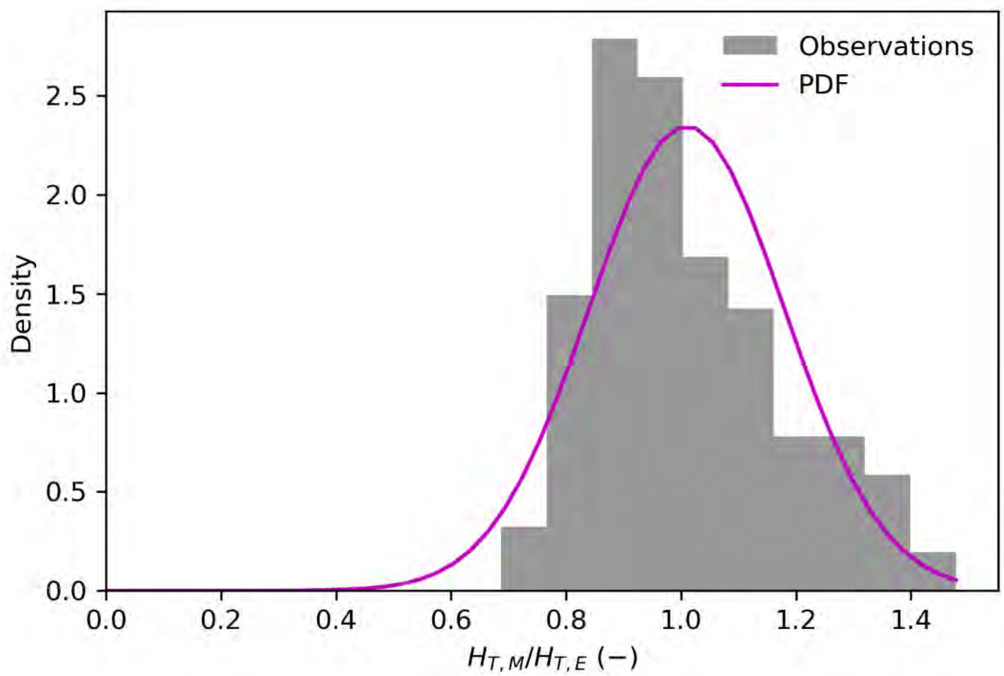

Figure A.4. Density histogram of the ratio of observations of height of the trees to the calculated value from the regression.

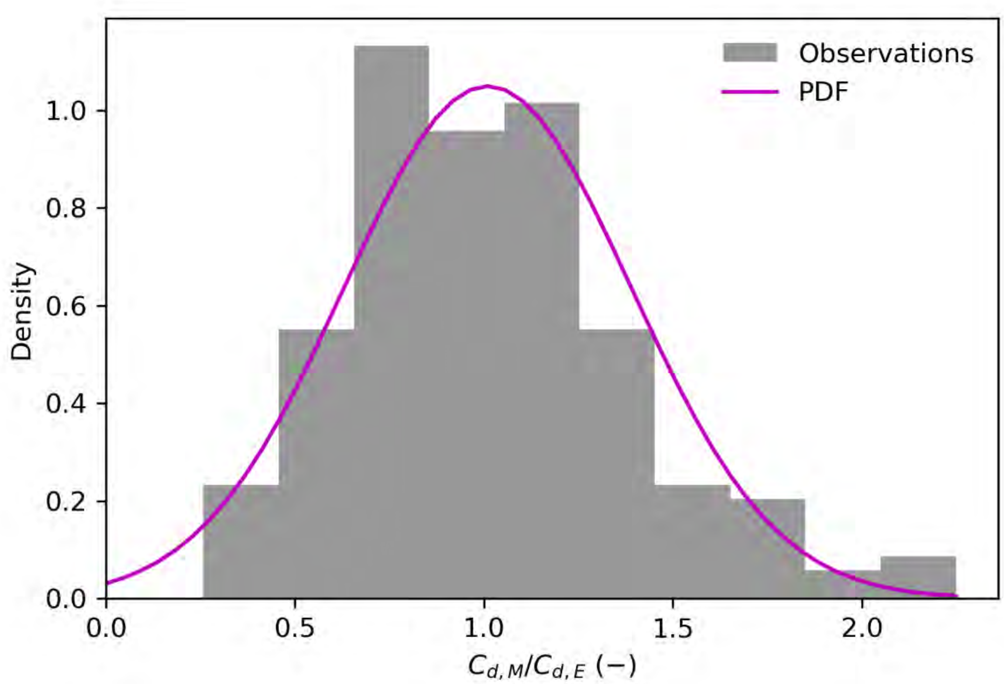

Figure A.5. Density histogram of the ratio of observations of drag coefficient to the calculated value from the equation in Kelty et al. (2022).

Appendix B. Model Grid

Different grid sizes within the mangroves were tested and evaluated, as in Section 3.3.2. The computational time was determined on an Intel(R) Xeon(R) CPU E3-1230 v5 @ 3.40 GHz. As the grid became finer, the expected overtopping and probability of failure decreased, converging to one value in each year of the design life (Figure B.1). Therefore, utilizing a coarser grid can be considered conservative. The grid size of Δx = 4 m was selected due to minimizing both the root mean square error and computational time (Figure B.2).

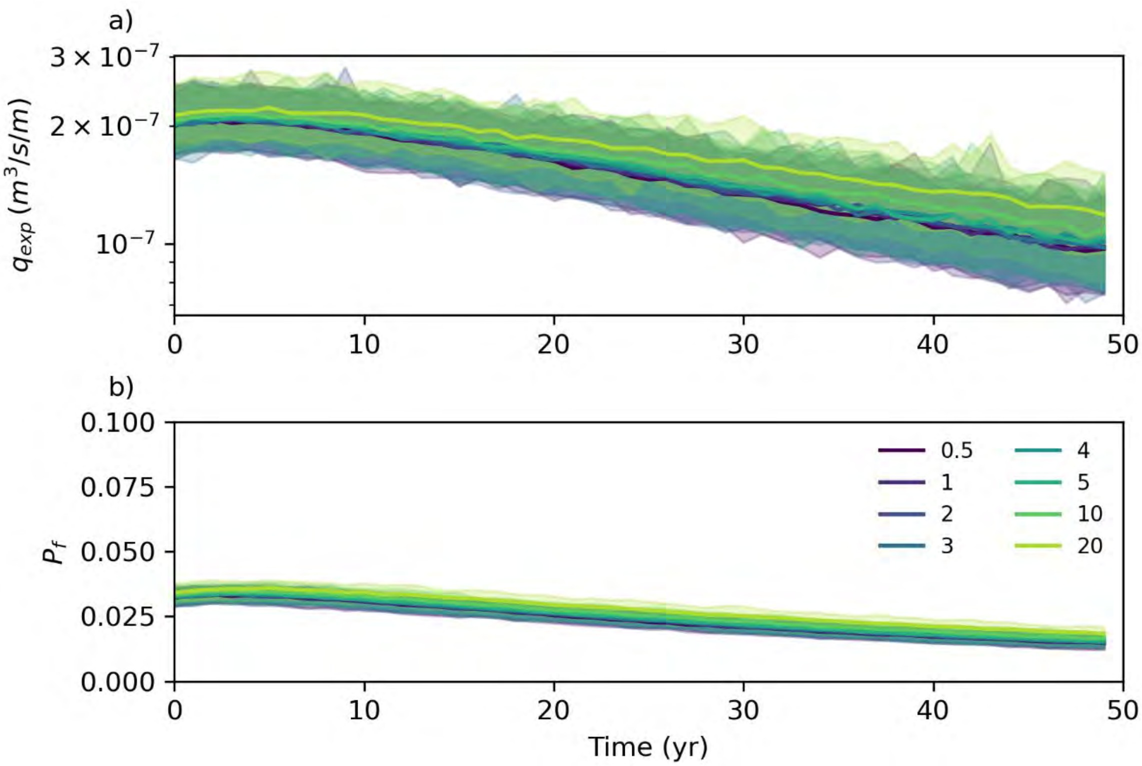

Figure B.1. a) Expected overtopping and b) probability of failure with 95% confidence intervals using grid cell sizes of Δx = 0.5 m, 1 m, 2 m, 3 m, 4 m, 5 m, 10 m, and 20 m, using 100 sets of 10,000 simulations.

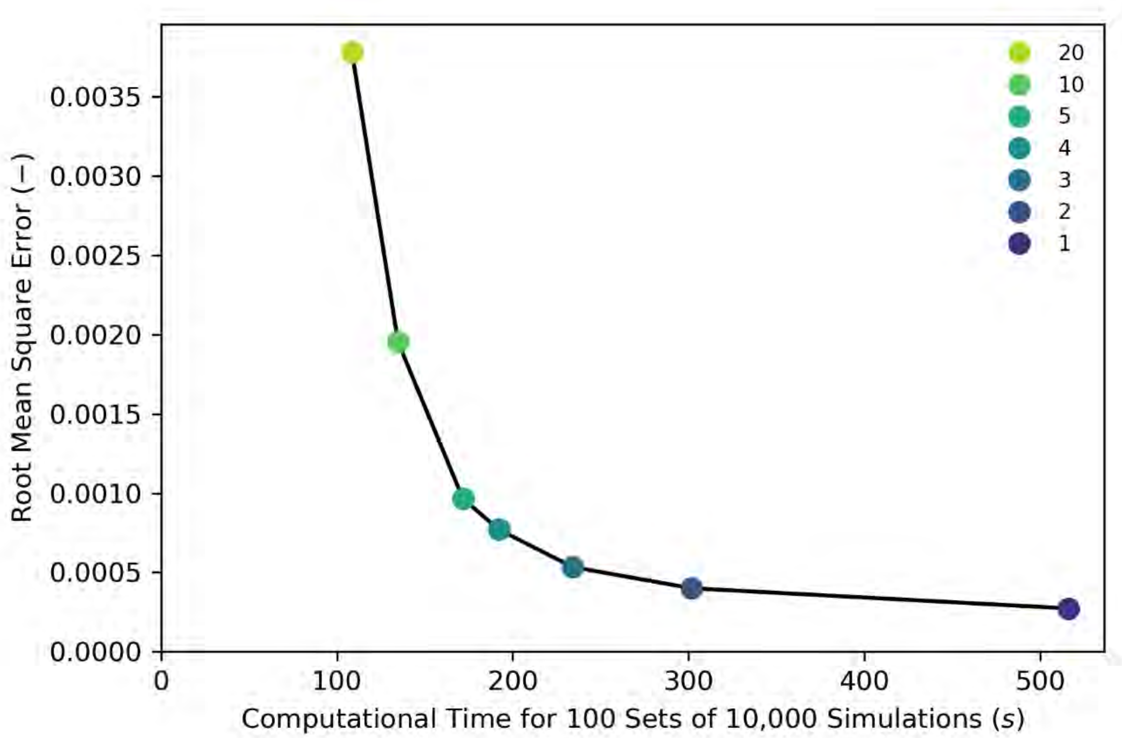

Figure B.2. Root mean square error vs. computational time for grid cell sizes of Δx = 1 m, 2 m, 3 m, 4 m, 5 m, 10 m, and 20 m, using 100 sets of 10,000 simulations. Root mean square error is calculated by comparing the result with the result using Δx = 0.5 m.

Appendix C. Monte Carlo Simulations

Different numbers of simulations and sets of simulations were evaluated as in Section 3.3.3. 10,000 simulations was chosen as a value that provides an adequate tradeoff between the coefficient of variation and computational time (Figure C.2). The coefficient of variation for the number of sets of simulations quickly converged for the probability of failure, so 100 sets of 10,000 simulations was chosen to minimize time (Figure C.3) and provide smooth confidence intervals around the probability of failure (Figure C.4). The total time to complete 50,000,000 computations between steps 2-6 was 194 seconds, or 3.2 minutes.

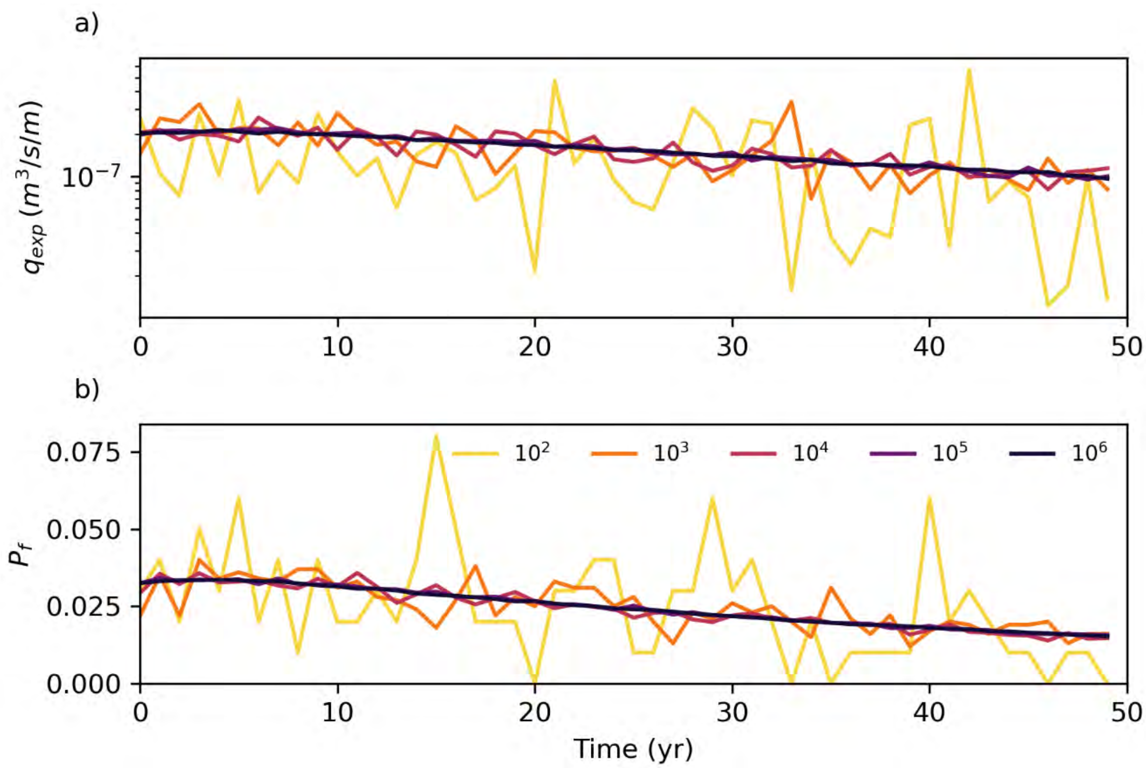

Figure C.1. a) Expected overtopping and b) probability of failure for 100, 1,000, 10,000, 100,000 and 1,000,000 simulations.

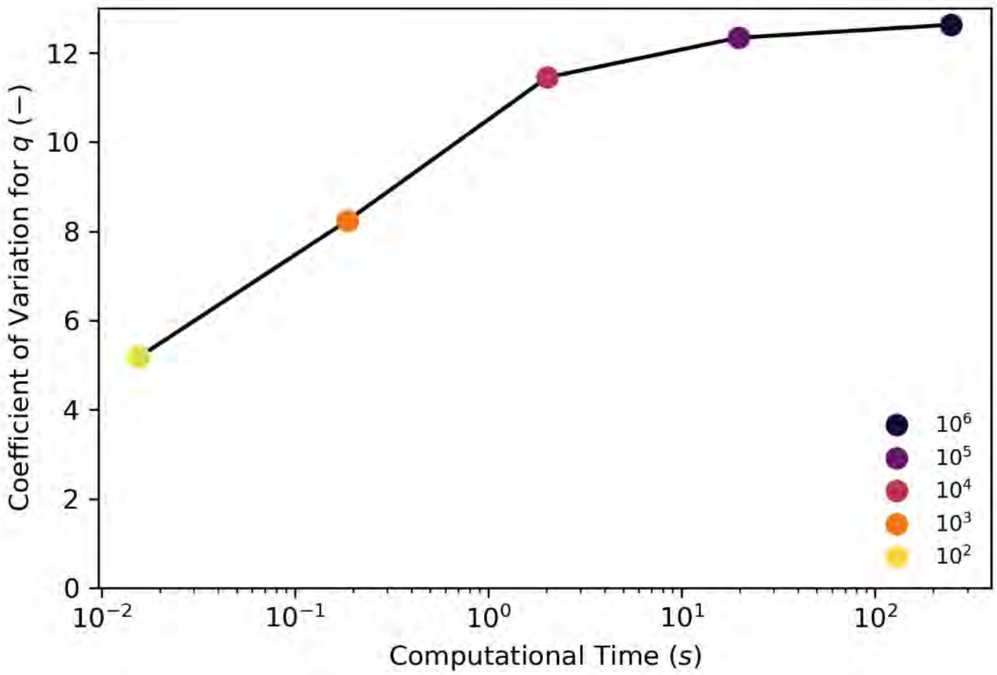

Figure C.2. Coefficient of variation for the expected value of overtopping for 100, 1,000, 10,000, 100,000, and 1,000,000 simulations as a function of computational time.

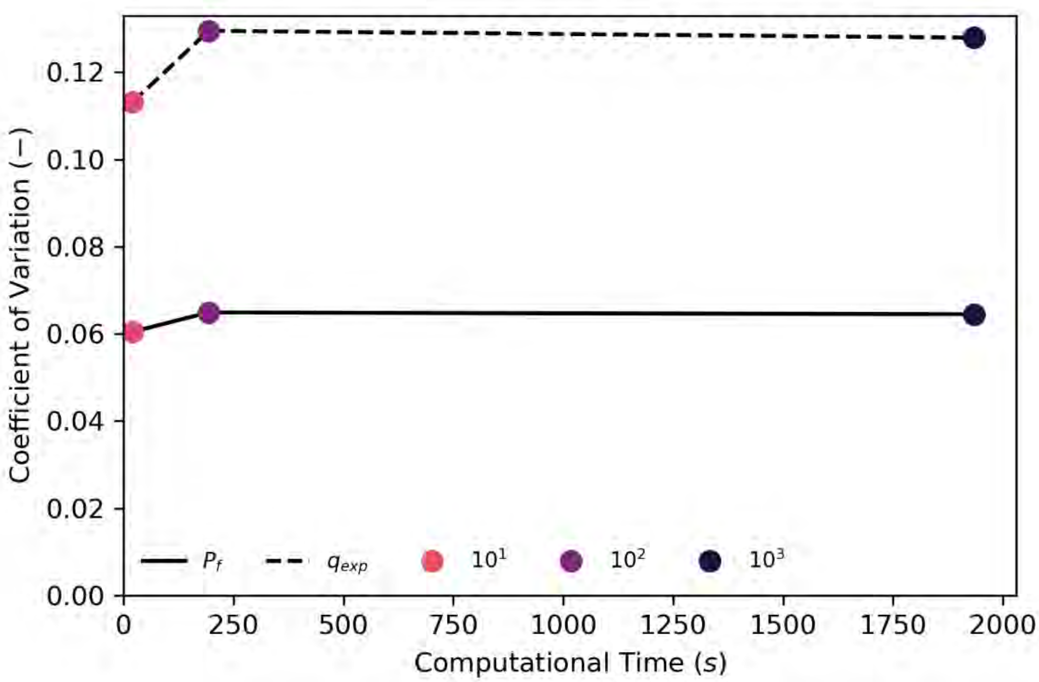

Figure C.3. Coefficient of variation vs. computational time for 10, 100, and 1,000 simulations, for both expected overtopping and probability of failure.

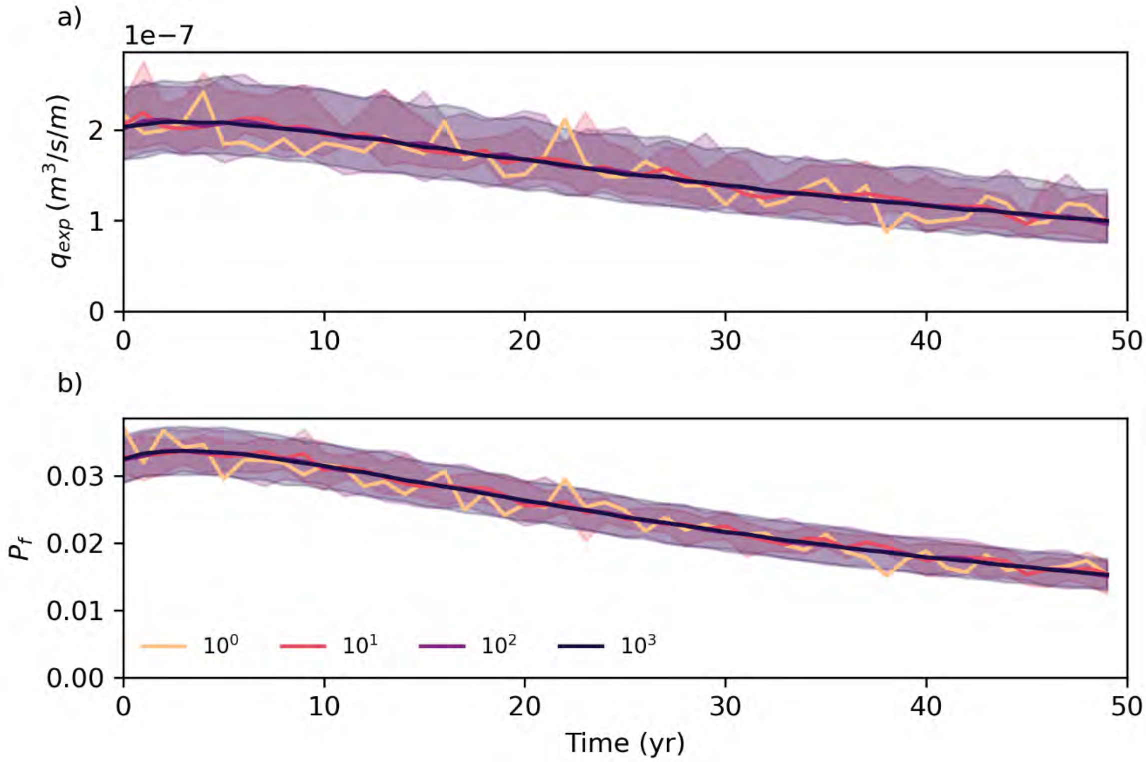

Figure C.4. a) Expected overtopping and probability of failure for 1, 10, 100, and 1,000 sets of 10,000 simulations with 95% confidence intervals, if applicable.

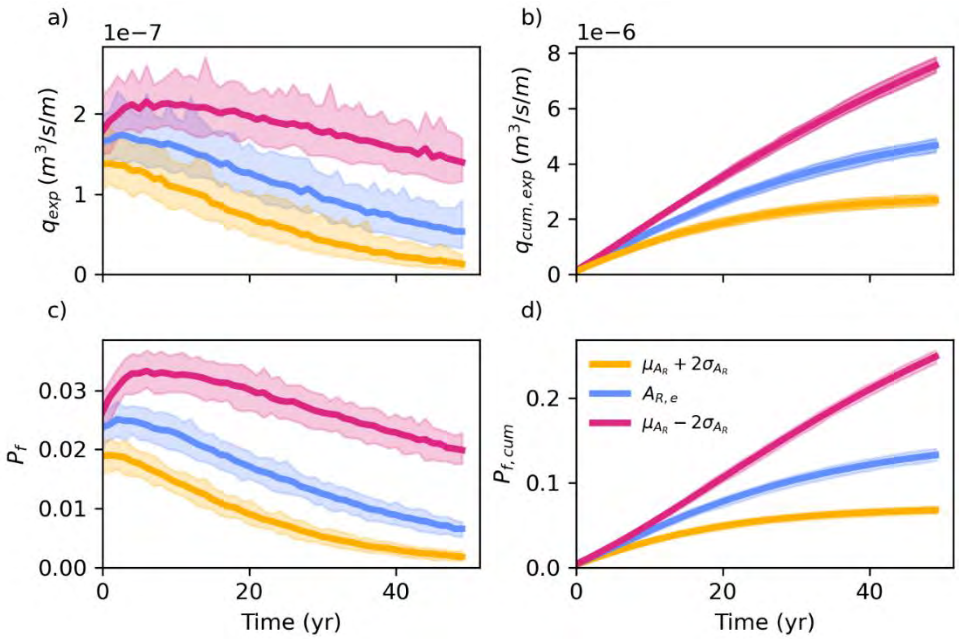

Figure D.1. Expected performance of the mangrove system for each year of the design life for three projected area of the roots relations, with a) the expected value of overtopping, b) the expected cumulative overtopping, c) the probability of failure due to overtopping, and d) the probability of failure due to cumulative overtopping with 95% confidence intervals.

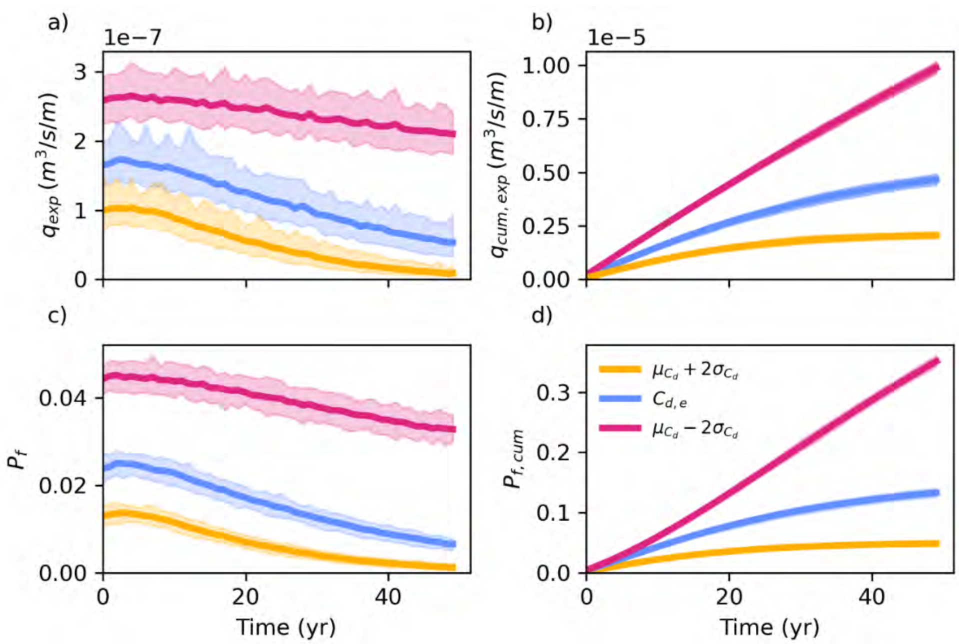

Figure D.2. Expected performance of the mangrove system for each year of the design life for three drag coefficient relations, with a) the expected value of overtopping, b) the expected cumulative overtopping, c) the probability of failure due to overtopping, and d) the probability of failure due to cumulative overtopping with 95% confidence intervals.

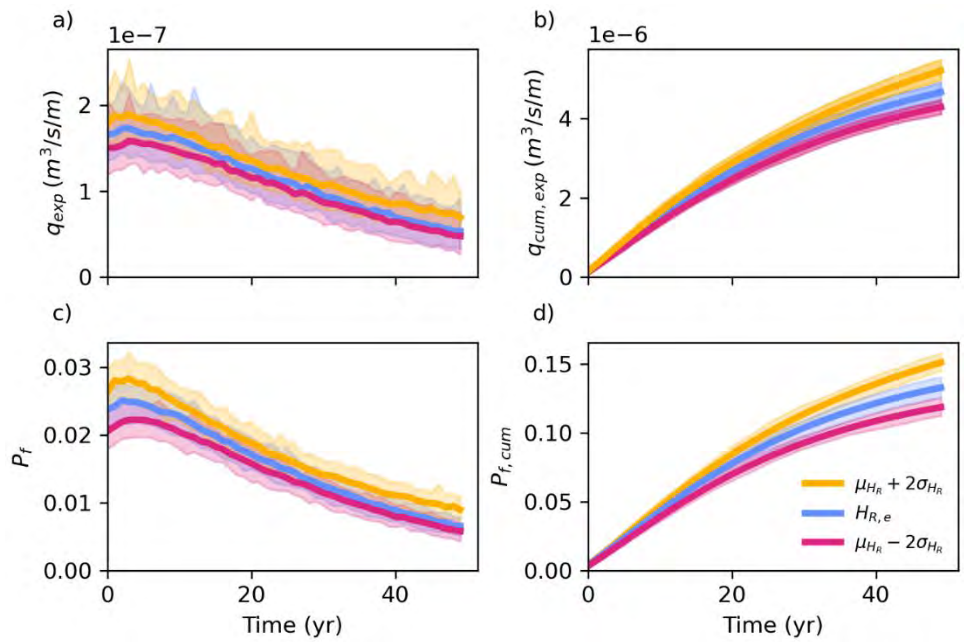

Figure D.3. Expected performance of the mangrove system for each year of the design life for three height of the roots relations, with a) the expected value of overtopping, b) the expected cumulative overtopping, c) the probability of failure due to overtopping, and d) the probability of failure due to cumulative overtopping with 95% confidence intervals.

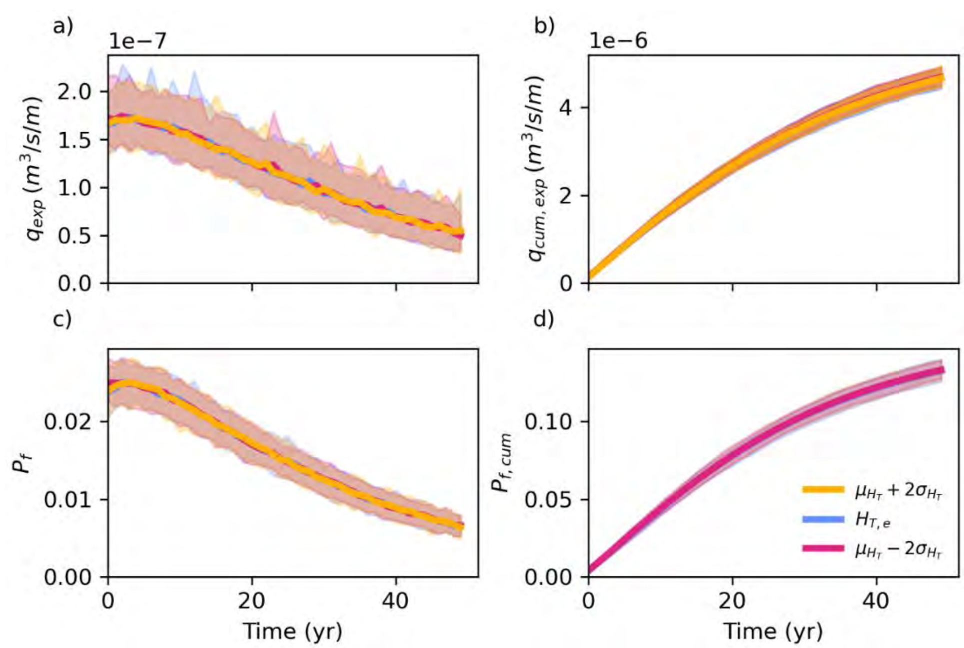

Figure D.4. Expected performance of the mangrove system for each year of the design life for three height of the trees relations, with a) the expected value of overtopping, b) the expected cumulative overtopping, c) the probability of failure due to overtopping, and d) the probability of failure due to cumulative overtopping with 95% confidence intervals.